FFI RAPPORT

LOCALIZATION OF A MERCHANT SHIP BY MEANS OF STRIATIONS IN A LOFARGRAM

SØSTRAND Knut A

FFI/RAPPORT-2005/00949

LOCALIZATION OF A MERCHANT SHIP BY MEANS OF STRIATIONS IN A LOFARGRAM

SØSTRAND Knut A

FFI/RAPPORT-2005/00949

FORSVARETS FORSKNINGSINSTITUTT
Norwegian Defence Research Establishment
P O Box 25, NO-2027 Kjeller, Norway

FORSVARETS FORSKNINGSINSTITUTT (FFI)
Norwegian Defence Research Establishment

P O BOX 25
N0-2027 KJELLER, NORWAY

UNCLASSIFIED

SECURITY CLASSIFICATION OF THIS PAGE
(when data entered)

REPORT DOCUMENTATION PAGE

1) PUBL/REPORT NUMBER	2) SECURITY CLASSIFICATION	3) NUMBER OF PAGES
FFI/RAPPORT-2005/00949	UNCLASSIFIED	63
1a) PROJECT REFERENCE	**2a) DECLASSIFICATION/DOWNGRADING SCHEDULE**	
FFI-IV/891/914	-	

4) TITLE

LOCALIZATION OF A MERCHANT SHIP BY MEANS OF STRIATIONS IN A LOFARGRAM

5) NAMES OF AUTHOR(S) IN FULL (surname first)

SØSTRAND Knut A

6) DISTRIBUTION STATEMENT

Approved for public release. Distribution unlimited. (Offentlig tilgjengelig)

7) INDEXING TERMS

IN ENGLISH:	IN NORWEGIAN:
a) Underwater acoustics	a) Undervannsakustikk
b) Waveguide invariant	b) Bølgeleder-invariant
c) Localization	c) Lokalisering
d) Lofargram	d) Lofargram
e) Antenna array	e) Array-antenne

THESAURUS REFERENCE:

8) ABSTRACT

In low frequency passive sonar a *lofargram* is a common presentation form for time varying spectral data. A target may emit narrow frequency lines and broadband noise. Depending upon the transmission channel, the target noise can show up as multipath interference patterns – *striations* - in the lofargram. These may be very consistent, and can for underwater waveguides be described mathematically by use of the so-called *waveguide invariant β*. Under some idealized circumstances, β is a compact characterization of the waveguide. Variable bathymetry can also be handled.

During an experiment in the Barents Sea, a passing tanker having a rich acoustical output gave a lofargram with many striations. These are successfully modelled by means of β. Inversely, parts of the lofargram can be used for localization of the target by way of the striations. The speed of the striation patterns along an array can be related to the target speed, taking account of the target's track with its offset and course in relation to the antenna axis. A method of speed estimation by means of mode filtering in frequency and direction is also treated. Auxiliary measurements with SUS explosive charges and a CW towing support the tanker results.

9) DATE	AUTHORIZED BY	POSITION
	This page only	
2005-04-06	Elling Tveit	Director of Research

ISBN 82-464-0932-8

UNCLASSIFIED

SECURITY CLASSIFICATION OF THIS PAGE
(when data entered)

CONTENTS

LOCALIZATION OF A MERCHANT SHIP BY MEANS OF STRIATIONS IN A LOFARGRAM

Executive summary

A *lofargram* is a kind of passive sonar display – on paper or on screen – of the frequency spectrum of a received sound signal as function of time. Vessels driven by machinery have acoustical *signatures*, i e certain combinations of frequency lines, from which the vessel can be identified or classified. By means of a hydrophone array the direction (bearing) of the vessel can be determined. Direct estimation of the target's range and speed is difficult, however, and is usually based upon indirect methods, such as observation of bearing changes over time.

Under certain sound propagation conditions, and if the vessel's lofar signature is "rich" enough, the lofargram can contain certain interference patterns – called *striations* – that run across frequency and time. These are due to multipath propagation, and can in theory be tied up with the distance to the vessel. The movements of the striations can be tied up with its speed. During an experiment in the Barents Sea in June 2003, 40 nautical miles north of Vardø, FFI had a 930 metres hydrophone array on the sea bottom. Opportunity had a tanker passing fairly close, and its acoustical output was registered on the hydrophone array. The tanker had a strong lofar signature with many frequency lines in addition to broadband noise. The striations were very prominent. This gave a good opportunity for testing the theory of striations in an interesting sea area.

Range. It turned out that the theoretical description and the measurements were in good accordance with each other. Certain ideal assumptions about the sound transmission conditions – the acoustical waveguide – had to be made. Knowledge of the bathymetry between target and receiving array was also necessary. The tanker's position was followed for about 100 kilometres.
Speed. The speed of a striation along the array can be measured. This speed is determined by the target's speed, its course in relation to the array axis, and the track's offset in relation to the array. Theory and measurements were also here in reasonable accordance with each other.

The experiment is a demonstration and confirmation of the applicability of striations for localization. This means that more localization information can sometimes be pulled out of a lofargram than what is usually done. The appropriateness of the theoretical descriptions seems established. How representative this is for other areas and other "targets" has not been evaluated, but the potential has been pointed out. If there is a need for acoustical surveillance of tanker traffic and the means are available, use of striations for localization is one of the tools in the box.

Abbreviations and symbols

CPA = closest point of approach
Lofargram = passive sonar spectrogram plot
RPM = revolutions per minute
Striation = interference pattern in lofargram
SUS = a type of explosive sound source

a = CPA distance
$d(r)$ = sea depth at range r
k_n = wavenumber for mode n
c = speed of sound
v = speed of target or source
α = bearing angle of array from source
β = waveguide invariant
θ = source-track angle relative to array axis
φ = grazing angle
ψ = bearing angle of source from array broadside

1 INTRODUCTION

A *lofargram* is a plot belonging to the passive sonar sphere, showing the time varying spectrum of a sound signal. Interference patterns (striations) in lofargrams have been observed for decades. Best known are maybe the patterns due to the Lloyd mirror effect, which concerns interference between direct and surface reflected sound, causing parabola-like patterns in a lofargram when a target is passing near the receiver. But interferences can also be observed at long ranges. Then the whole collection of modes in the underwater waveguide comes into play. In recent years a theoretical treatment of striations in terms of a certain *waveguide invariant* β have appeared. The origin was a work by S. D. Chuprov published in 1982 (1). Since the late 1990s several papers concerned with this subject have been published in the open western literature (2), (3), (4).

A key element in this theory is the formulation of striation patterns as functions of range, frequency and waveguide parameters. The task, after observing a striation in a lofargram to find the range, is something else, and has not necessarily a unique answer. The task becomes easier with increasing observation length. Alone or together with other observables (bearing, doppler), the striations can be contributive in updating a target's position and track.

During the period June 3-16, the acoustic experiment Phase S-IIIb of project SWASI-III (5) was conducted by FFI in the Barents Sea, approximately 40 nautical miles north of Vardø. The receiver was an experimental array consisting of a vertical and a horizontal section (L-shaped array) deployed in 280 m of water, with the horizontal section at the bottom. Sound sources were a towed projector, SUS charges, airgun, imploding light bulbs, and targets of opportunity. Of relevance for the present report is the horizontal part of the array, using 20 hydrophones over 930 m, oriented NW - SE.

During the afternoon of June 8th 2003 a target of opportunity came by, moving from east to west. This was a tanker of relatively modest size, but it had a rich acoustic signature containing many sharp harmonic lines over a wide frequency band, in addition to broadband noise. The lofargram, which will be shown below, contains a multitude of striation patterns. These will here be related to the theoretical descriptions. Using sections of the patterns for determining target range and speed will be done. Figure 1.1 shows a map over the experimental area, the tanker track, and the tracks of some supporting measurements.

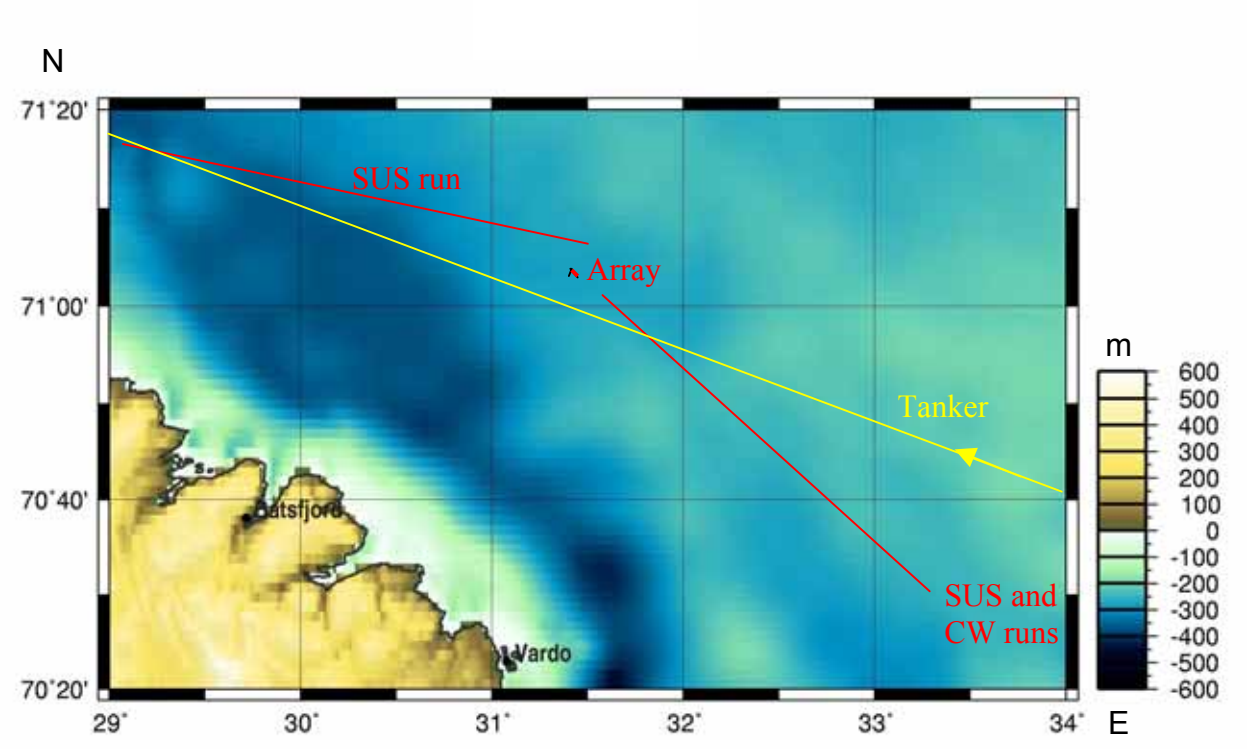

Figure 1.1 Experimental area with array position and tracks
Yellow track: tanker target
Red tracks: SUS runs, 40 Hz CW run, bottom profiles

In Chapter 2 the lofar tanker signature is introduced and the striations identified. Chapter 3 presents the theory of striations in terms of the waveguide invariant β. The target "ground truth" is established in Chapter 4, based upon measurements independent of the striations, in this case changes in doppler and bearing plus radar fix. The striation theory is applied to the target lofargrams in Chapter 5, and a small localization "exercise" is conducted. Relating the target speed to striation speed along the array is treated in Chapter 6, and the influence of varying bathymetry, skew track and track offset is found. Chapter 7 gives an alternative method of speed determination by doppler and angle of modes. Appendix A gives a more detailed presentation of the target signature. In Appendix B the waveguide invariant β measured by way of explosive sound sources is described. Appendix C contains a more detailed discussion about the harmonics and striations. In Appendix D speed estimates using a 40 Hz towed source are given.

2 LOFARGRAM WITH TANKER SIGNATURE

Figure 2.1 is a lofargram, showing the time varying spectrum of a hydrophone signal over 3 hours of the relevant period. The frequency resolution is 0.05 Hz. The spectra are computed by FFT with Hanning weighting, a total of about 680 for the whole page. The tanker signature dominates the picture almost completely. A few exceptions are some horizontal stripes due to instrument noise, some broad vertical lines in the lower and upper parts, probably due to other ships. There are also a few narrow lines that do not belong to the tanker. Two kinds of patterns are prominent

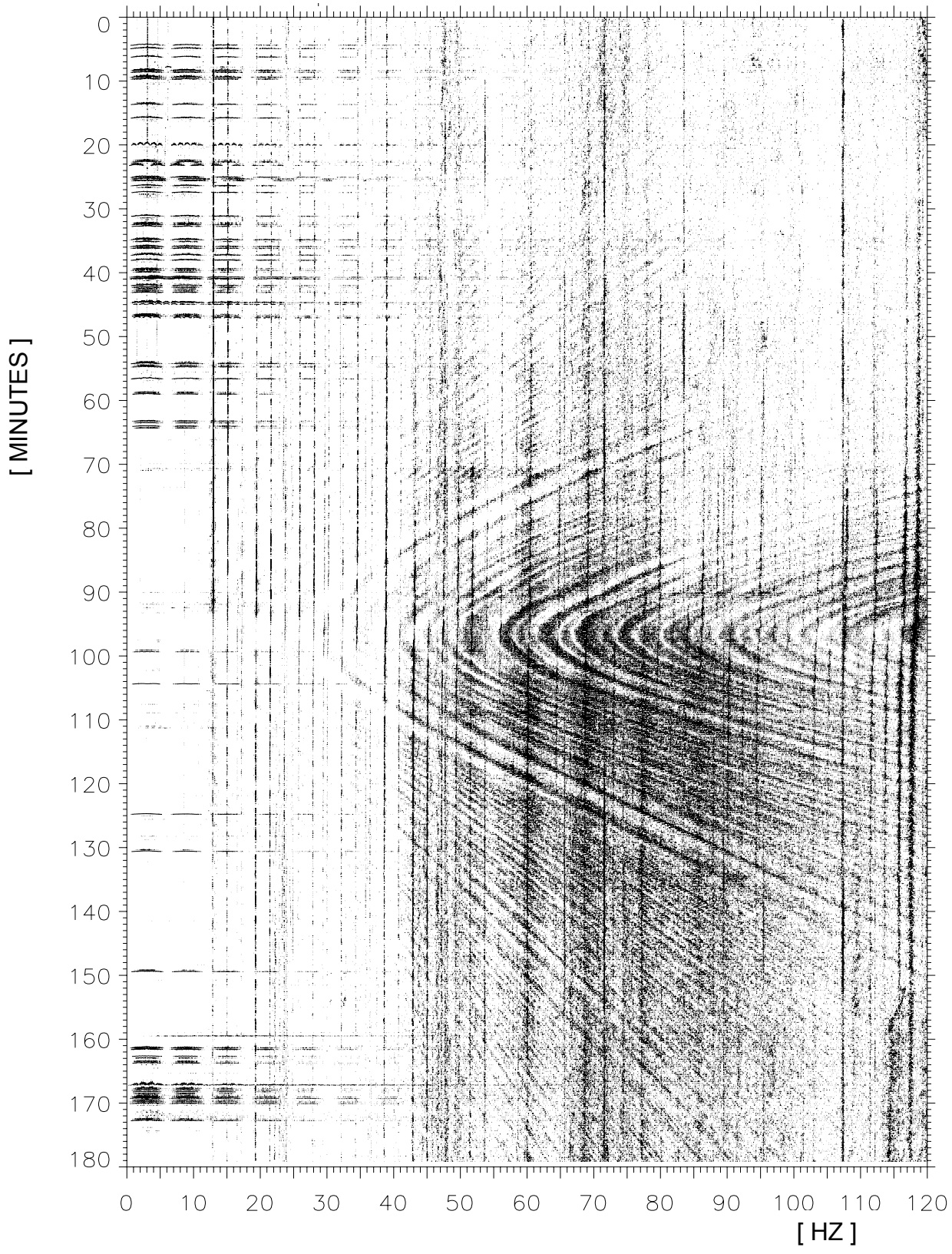

Figure 2.1 Lofargram showing passage of target at CPA-time 97 minutes (relative time). Frequency resolution = 0.05 Hz

(a) A set of vertical lines
(b) A set of parabola-like patterns centered on a horizontal axis at time 97 minutes.

Pattern (a) consists mainly of a set of harmonics with $f_0 = 2.15$ Hz as the fundamental. Not all harmonics are visible, neither the fundamental. There are also a few lines belonging to the tanker that are unrelated to f_0.

Pattern (b) is due to interference between multipaths of the target's harmonics and broadband noise. The mechanism is the following. The received signal in a FFT slot can be taken as a sum of sine waves from propagation paths having slightly different lengths, because of their vertical angles. As the range changes, the phases of the sine waves will change at different rates, thereby creating varying interference maxima and minima. The positions of these extrema are range and frequency dependent, but exhibit fairly consistent patterns. These patterns are the *striations*. The axis of the striation "parabolas" is located at the time when the target is closest to the hydrophone, called CPA (closest point of approach).

A more detailed discussion of the target signature with reference to ship and machinery is given in Appendix A.

3 THEORY OF STRIATIONS

3.1 The beta connection

In current literature, striation patterns in lofargrams are usually treated mathematically using the *waveguide invariant β*. This leads to compact expressions. The basic development has some elegance and will be shown here, mainly following (2) and (3). The striation patterns as functions of range and frequency will be found. The characteristics of the propagation channel are all assumed contained in β.

The waveguide equation, well known from textbooks, can be written

$$p(\omega) = \sum_m \sqrt{2\pi}\, \frac{exp(-jk_m r)\, \Psi_m(z)\, \Psi_m(z_s)}{\sqrt{k_m r}} \equiv \sum_m A_m\, exp(-jk_m r) \tag{3.1}$$

The meaning of the different terms will be assumed known. The received *power* at a particular range and frequency will be proportional to

$$I(\omega) = |p(\omega)|^2 \approx \sum_m |A_m|^2 + \sum_{m \neq n} A_m^* A_n\, exp(\, j(k_m - k_n)r\,) \tag{3.2}$$

The aim now is to find patterns of extrema of this function in the frequency-range plane (the wavenumbers k are functions of frequency). Consider for the moment only two modes m and

n, and ignore the slowly-varying amplitudes A_m and A_n. Along an extremum in the ω-r plane the *phase* will be constant, such that

$$\partial\left((k_m - k_n)r\right) = \left(\frac{dk_m}{d\omega} - \frac{dk_n}{d\omega}\right) r\, d\omega + (k_m - k_n)\, dr = 0 \tag{3.3}$$

Rearranging,

$$\frac{\dfrac{d\omega}{\omega}}{\dfrac{dr}{r}} = -\frac{\dfrac{k_m}{\omega} - \dfrac{k_n}{\omega}}{\dfrac{dk_m}{d\omega} - \dfrac{dk_n}{d\omega}} \tag{3.4}$$

The textbook phase and group speeds, respectively, are given by

$$v_m = \frac{\omega}{k_m} \qquad u_m = \frac{d\omega}{dk_m} \tag{3.5}$$

The *waveguide invariant* β introduced by S. D. Chuprov in 1982 (1) is defined thus,

$$\beta = -\frac{\dfrac{1}{v_m} - \dfrac{1}{v_n}}{\dfrac{1}{u_m} - \dfrac{1}{u_n}} \tag{3.6}$$

Then from Equation (3.4)

$$\frac{d\omega}{dr}\,\frac{r}{\omega} = \beta \tag{3.7}$$

In a range-independent waveguide the invariant β is *constant* for all pairs of modes and over all frequencies. In other words, in the equation above the left side is constant and the same for all mode combinations. Integrating this differential equation gives

$$\omega = \omega_o \left(\frac{r}{r_o}\right)^{\beta} \tag{3.8}$$

This expresses the striation pattern in the ω-r plane. (ω_o, r_o) is a point which the pattern goes through, a convenient way of incorporating the integration constant. Here ends the basic development.

3.2 The range-time connection

In an ideal, flat waveguide, β=1 (2). In that case

$$\omega = \frac{\omega_0}{r_o} r \tag{3.9}$$

In order to go from a range versus frequency diagram to a time versus frequency diagram (lofargram), knowledge or assumptions about the movement of the target is needed. In the simplest case, the target is moving at constant course and speed straight towards or away from the receiver. Then range is proportional to time, and the striations in a lofargram will under the $\beta = 1$ condition be straight lines through the point $(\omega, r) = (0, 0)$. This is illustrated in Figure 3.1.a.

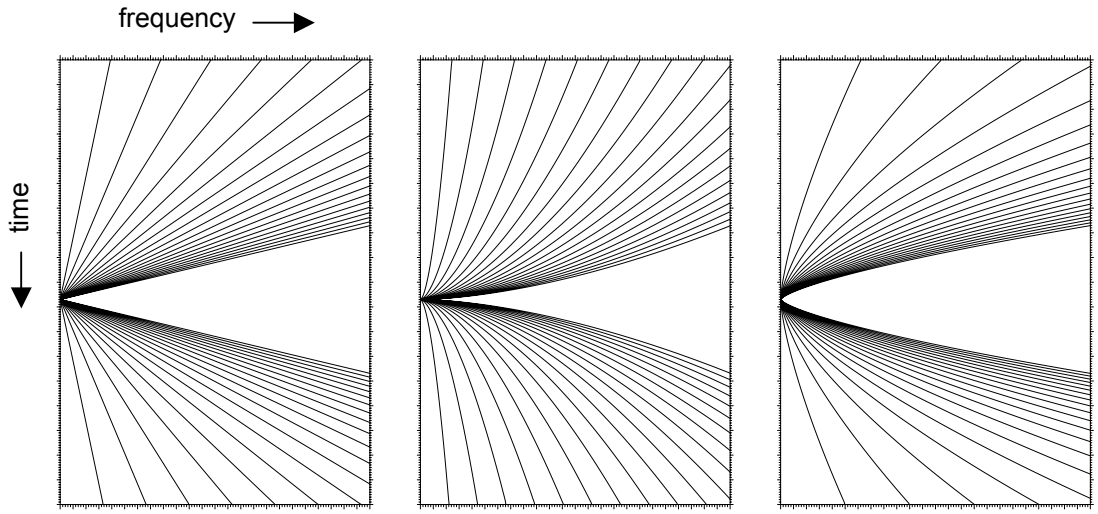

(a) CPA=0 β=1 (b) CPA=0 β=0.6 (c) CPA=0 β=1.4

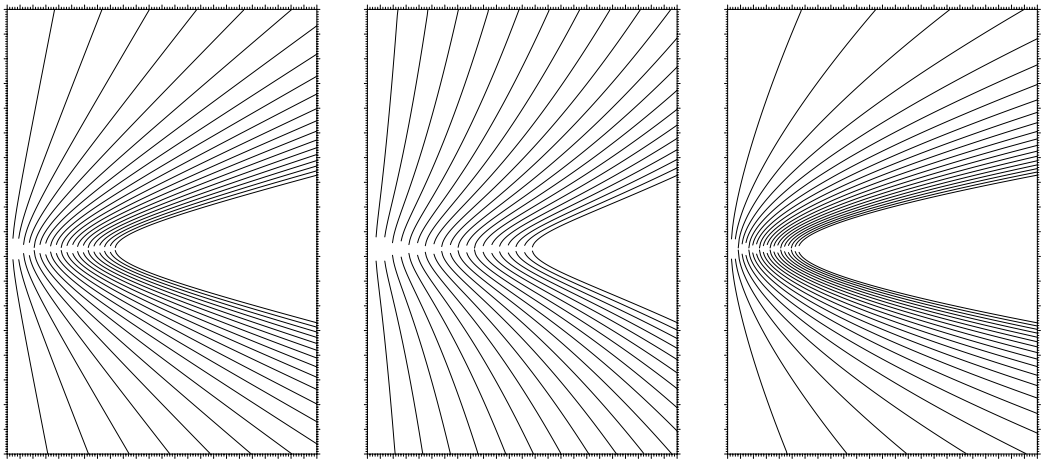

(d) CPA=5 km β=1 (e) CPA=5 km β=0.6 (f) CPA=5 km β=1.4

Figure 3.1 Theoretical striation patterns for different CPA distances and β values. Axes are as in Figure 2.1

Values of $\beta \neq 1$ will change the patterns. $\beta < 1$ will steepen them whereas $\beta > 1$ will flatten them as shown in Figures 3.1.b and c. If the target track is somewhat aside from the receiver, with shortest distance CPA = a and target speed = v, the relation between range and time becomes

$$r = \sqrt{a^2 + (vt)^2} \tag{3.10}$$

giving

$$\omega = \frac{\omega_0}{r_0}\sqrt{a^2 + (vt)^2} \tag{3.11}$$

This is for β = 1 shown in Figure 3.1.d. By a first glance the patterns can seem quite similar to the patterns in the lofargram Figure 2.1. Figures 3.1.e and f show β < 1 and β > 1, respectively.

Estimation of a ship's speed can sometimes be made from prior knowledge, with identification of its shaft rate or RPM from the lofargram. A direct method of speed estimation based upon striations will be given in Chapter 6. A somewhat different approach will be treated in Chapter 7.

4 TARGET GROUND TRUTH

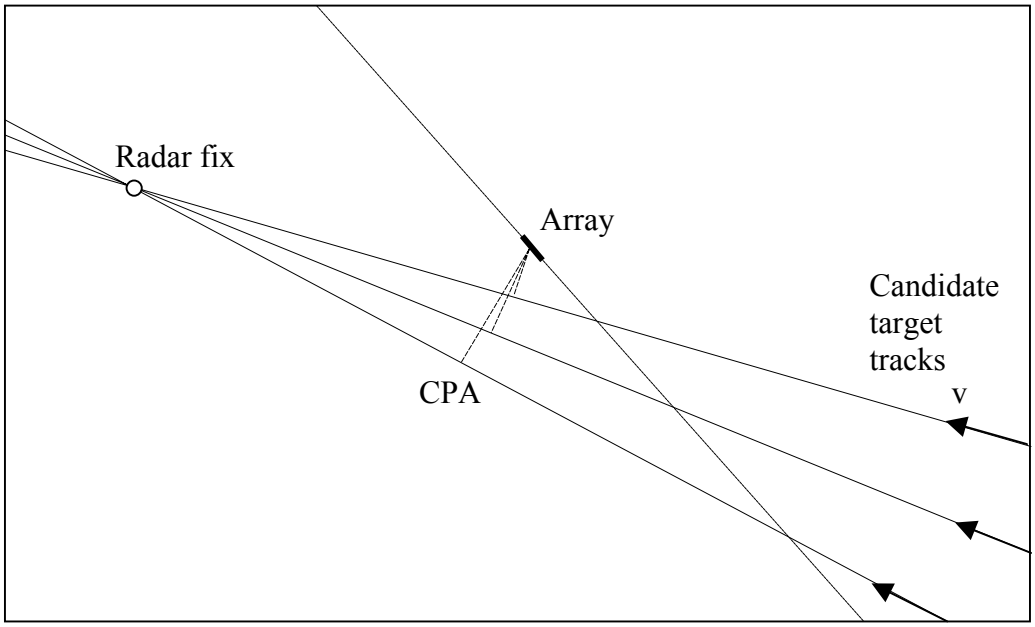

Figure 4.1 Array with axis. Three candidate target tracks with different CPAs, all going through the same radar fix

As this study is concerned with finding target position and speed by means of striations, it is necessary to have the "ground truth" for the target's track. This can be obtained from navigation or radar, or next best, an independent acoustical estimate of the target's movements. As the complete target passage is recorded on the bottom array, a target track can be established "after the event", independent of the striations, based upon changing bearings and

doppler shifts. Additional information are radar observations, which unfortunately were scarce, only one good and one uncertain.

The target is assumed to be moving at constant course and speed, Figure 4.1. Here are shown three track candidates, having different CPAs. The tracks are "anchored" in the (good) western radar observation, taken from the research vessel. The target's potential speed and course can now be varied to fit the measured bearing and doppler changes.

4.1 Beam-time diagrams

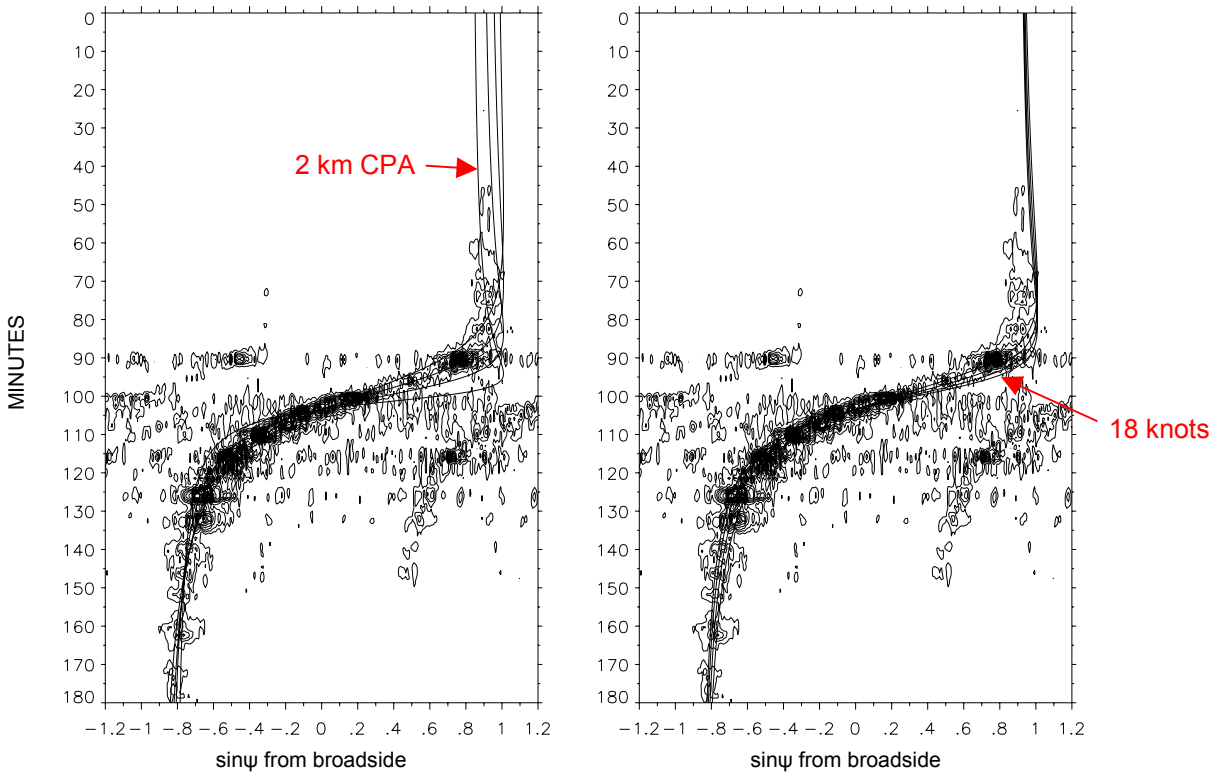

(a) Speed=15 knots CPA=2,4,6,8 km (b) Speed=12,14,16,18 knots CPA=5 km

Figure 4.2 Beam-time diagrams at 59.6 Hz with candidate tracks. ψ = target bearing angle. Contour plot is target signature.

Figure 4.2 shows sample beam-time diagrams over 3 hours at frequency 59.4 Hz. The underlying contour plots show how the target proceeds from near endfire east with $\sin\psi \approx 0.9$ to near endfire west with $\sin\psi \approx -0.8$.

In the left diagram the continuous lines correspond to $v_{tgt} = 15$ knots and CPA = 2, 4, 6, 8 km. They are found by simple geometry based upon Figure 4.1. In determining which line should be settled for, some consideration had to be given to where in relation to the signal signature the theoretical pattern should lie, in the center or near one edge. Modes can be thought of as up-and-down going rays. Their apparent bearing angle will always be less than the bearing of a direct ray, here represented by the continuous line. The theoretical line should therefore ideally lie just outside the high-angle part of the measured signature. This is the ideal situation. In

practice this has to be modified, remembering the non-zero widths of the beams. A fit here is therefore settled for when the theoretical lines lie just inside the outer edge. This is the case for CPA in the range 4 - 8 km.

In the right diagram the speed is varied, v = 12, 14, 16, 18 knots with CPA = 5 km. The differences are small, but 14 – 18 knots seems reasonable.

4.2 Doppler-time diagrams

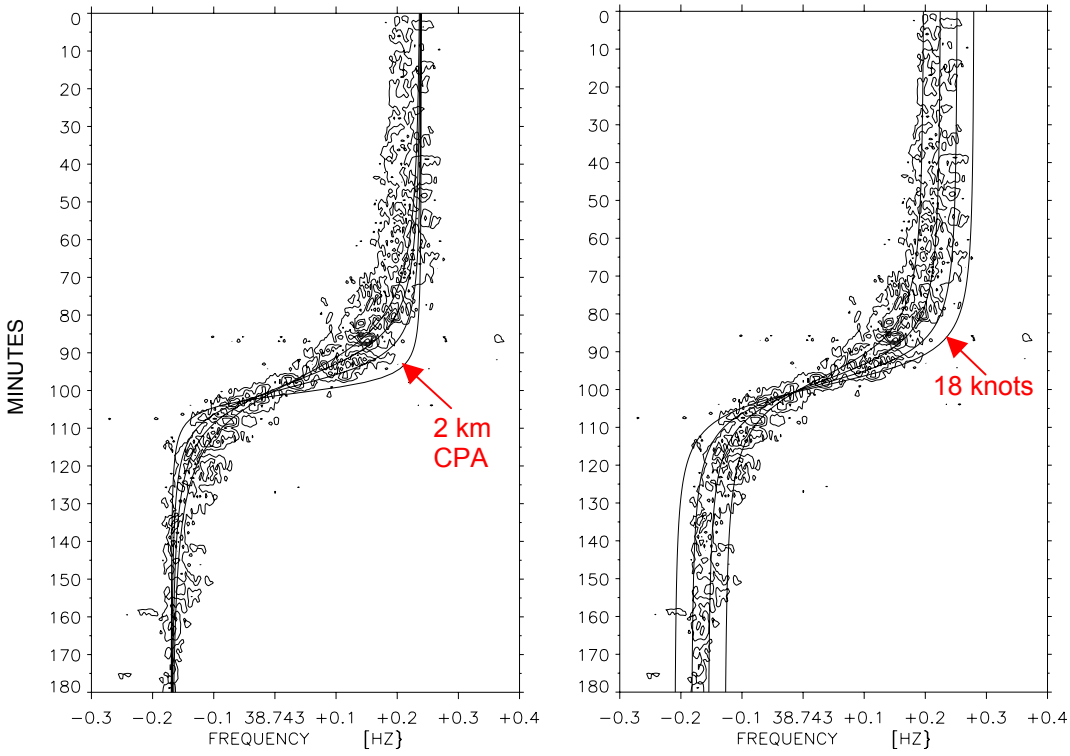

(a) Speed=15 knots CPA=2,4,6,8 km (b) Speed=12,14,16,18 knots CPA=5 km

Figure 4.3 Doppler-time diagrams at 38.7 Hz with candidate tracks. Contour plot is target signature.

Figure 4.3 gives sample high-resolution frequency-time diagrams around 38.7 Hz. It shows how the target proceeds from positive doppler east to negative doppler west. The doppler shift of a mode will always be less than the doppler of a direct ray, here represented by the continuous line. The theoretical line should ideally lie near the high-doppler part of the measured signature. For the reason of filters having non-zero bandwidth, a fit here is settled for when the theoretical lines lie just inside the outer edge. The left diagram gives CPA changes, the right diagram speed changes. Here CPA = 4 – 6 km and v = 14 –16 knots seem to give reasonable fit.

4.3 Discussion

It will be evident that the "truth" here has some tolerance. One cannot aim for extreme accuracy by this method. As mentioned there is the question about how the best match between theory and data should be done. There are possibilities for refinements. A simulation study might be useful. The examples here are for one frequency only. Several frequencies might be considered.

A different cause for possible reduced accuracy is that the target may have made a slight change of heading at time 91 minutes, as can be seen from Figure 1.1. Such a change has not been taken into account here.

A second radar observation (uncertain) was made when the target was close to the receiver. The tracks indicated above do not contradict this observation.

5 CONFIRMATION AND ESTIMATION

It is convenient here to treat range before speed, because certain features are better explained in the range context. In the meantime, the speed of the target will be assumed to be 15 knots. The striations will in the lofargrams be compared to those predicted by Equation (3.8). Three cases will be treated

(i) target east of the array
(ii) target west of the array, until 40 km
(iii) target west of the array, beyond 40 km

As will be shown later, the sea depth is slightly shallowing eastwards in Case (i) and slightly increasing westwards in Case (ii). A flat, ideal waveguide will then be assumed with $\beta = 1$. In Case (iii) westwards the bottom is more sloping downhill. It is then expected that $\beta > 1$. How to compute β from the bathymetry is shown in Appendix B.

The target is initially expected to pass fairly close to the receiver. Straight-line patterns like those in Figure 3.1.a will first be tried. This method is illustrative, and easy to use manually.

5.1 Target east of the array

Figure 5.1 shows a lofargram for this part of the run. The time axis has been expanded compared to Figure 1.1. In order to enhance the striations, this is not a single-hydrophone diagram, but a diagram from a tracking beam, a so-called *scissorgram* (3). Using beams as inputs to lofargrams does not change the patterns of the striations, but improves the signal to noise ratio.

Assume now that that the target has reached time 60 minutes, and that the lofargram can be observed up to this point. Put a straight line (shown in blue) along one of the striation patterns. This crosses the time axis at time 101 minutes. Expected time until CPA is then 101-60=41 minutes. At 15 knots this gives a range estimate of 19.0 km. True CPA appears at 97 minutes. The estimation error is then 4 minutes or 1.9 km. A more systematic application of the straight-line method will be demonstrated in Section 5.5.

When it becomes clear because of curved striations that the target will pass the receiver at a non-zero CPA (still assuming $\beta = 1$), several templates similar to Figure 3.1.d for different CPA offsets can be tried. One should use the longest observation time available. This is of course a more laborious procedure, but can be made electronically. A few template patterns (red colour) are shown in Figure 5.1 for CPA=6 km. The striation template method gives in fact a sharper estimate of the CPA distance than the beam-time and doppler-time methods of Chapter 4. Range estimates using curved-line templates will also be demonstrated in Section 5.5.

5.2 Target west of the array, first part

Figure 5.2 shows a lofargram for the target moving westwards, together with template patterns. It can be observed that the striation patterns at the later part of the diagram tend to curve downwards from the red lines. Clearly the theoretical model with $\beta = 1$ does not apply well there. Considering Figure 3.1.e, having $\beta < 1$ will make the theoretical striations curve more in the right direction. By trial and error, CPA = 6 km and $\beta = 1$ for the first 2/3 of the lofargram (red), and $\beta = 0.8$ for the last 1/3 (blue), were found to confirm well. Operating with several β values different from 1.0 of course calls for a more extensive set of templates.

5.3 Target west of the array, second part

Figure 5.3 shows a lofargram for this part, spanning 1½ hour. Patterns according to CPA = 6 km and $\beta = 0.8$ are indicated, and gives a reasonable fit.

5.4 A beta puzzle

A question is now if there are physical grounds for assuming $\beta < 1$ for the last part of the western run. As mentioned at the outset, $\beta > 1$ was expected. In Appendix B actual measurements of β by way of SUS charges are described, and theoretical predictions are also given. The measurements give $\beta \approx 1$ and the theory $\beta \approx 1.2$ at 80 km west. Both types of measurement – ship and SUS – points away from theory, but in the same direction. The theory as given assumes a constant sound speed profile in the water. On the other hand, the actual sound speed profile forms an internal sound channel. That can be the cause of the discrepancy. Both reflected and refracted modes can then be present. This could have considerable influence upon β. For details it is referred to Appendix B.

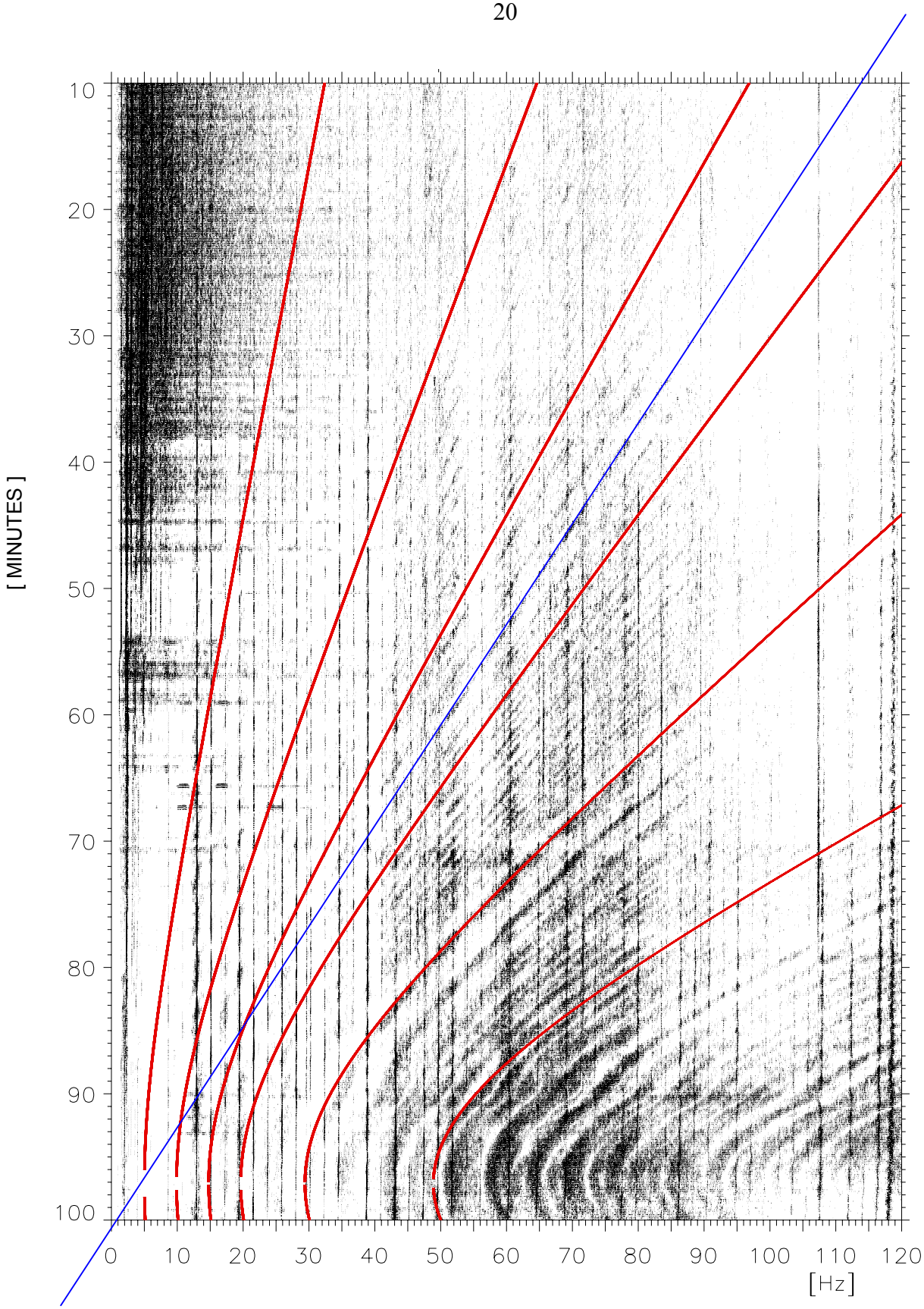

Figure 5.1 Lofargram for eastern run. Frequency resolution 0.05 Hz.
Assumed target speed 15 knots.
Blue line: striation pattern with CPA = 0 and $\beta = 1$
Red lines: striation patterns with CPA = 6 km and $\beta = 1$

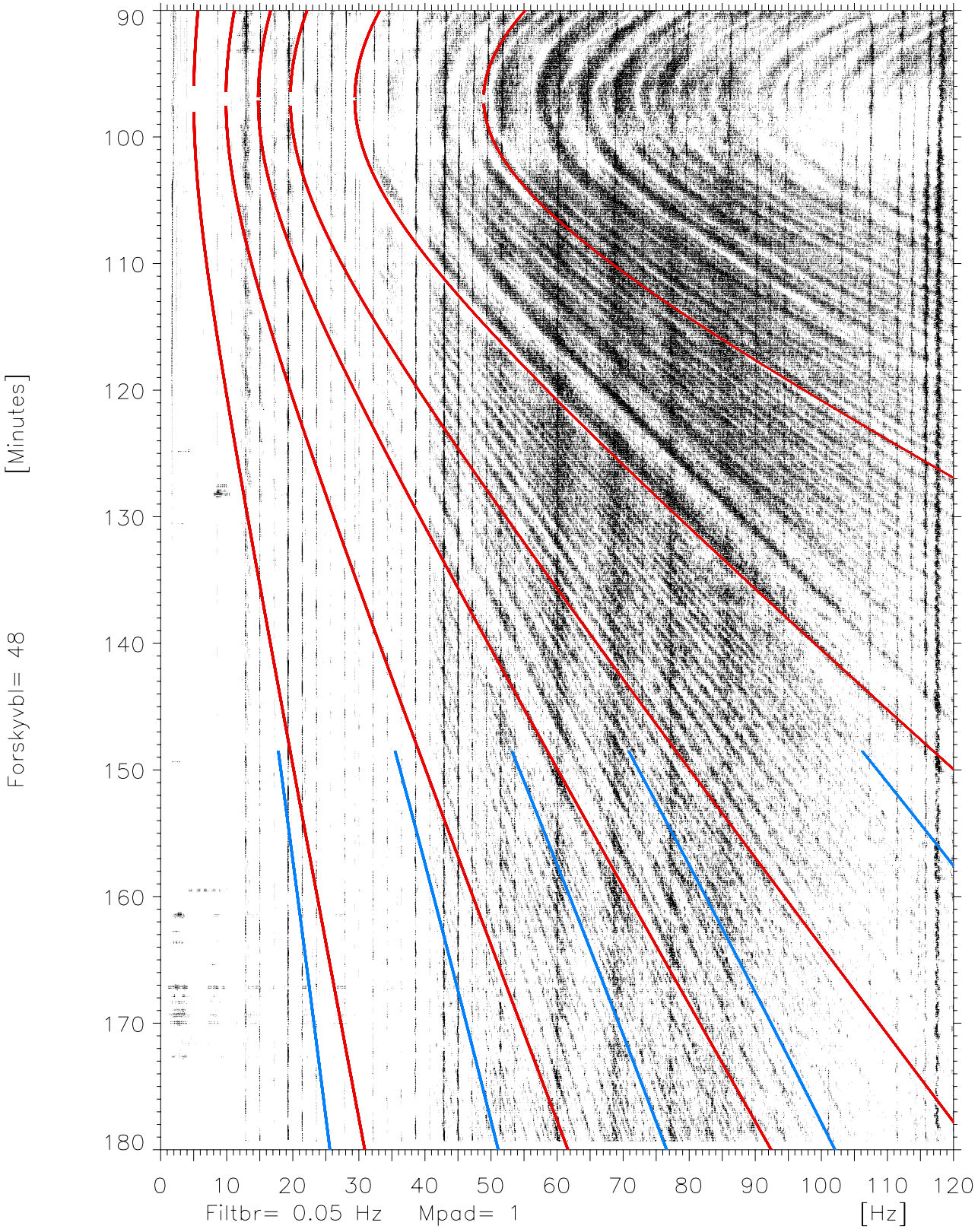

Figure 5.2 *Lofargram for western run, first part. Frequency resolution 0.05 Hz. Assumed target speed 15 knots.*
Red lines: striation patterns with CPA = 6 km and $\beta = 1$
Blue lines: striation patterns with CPA = 6 km and $\beta = 0.8$

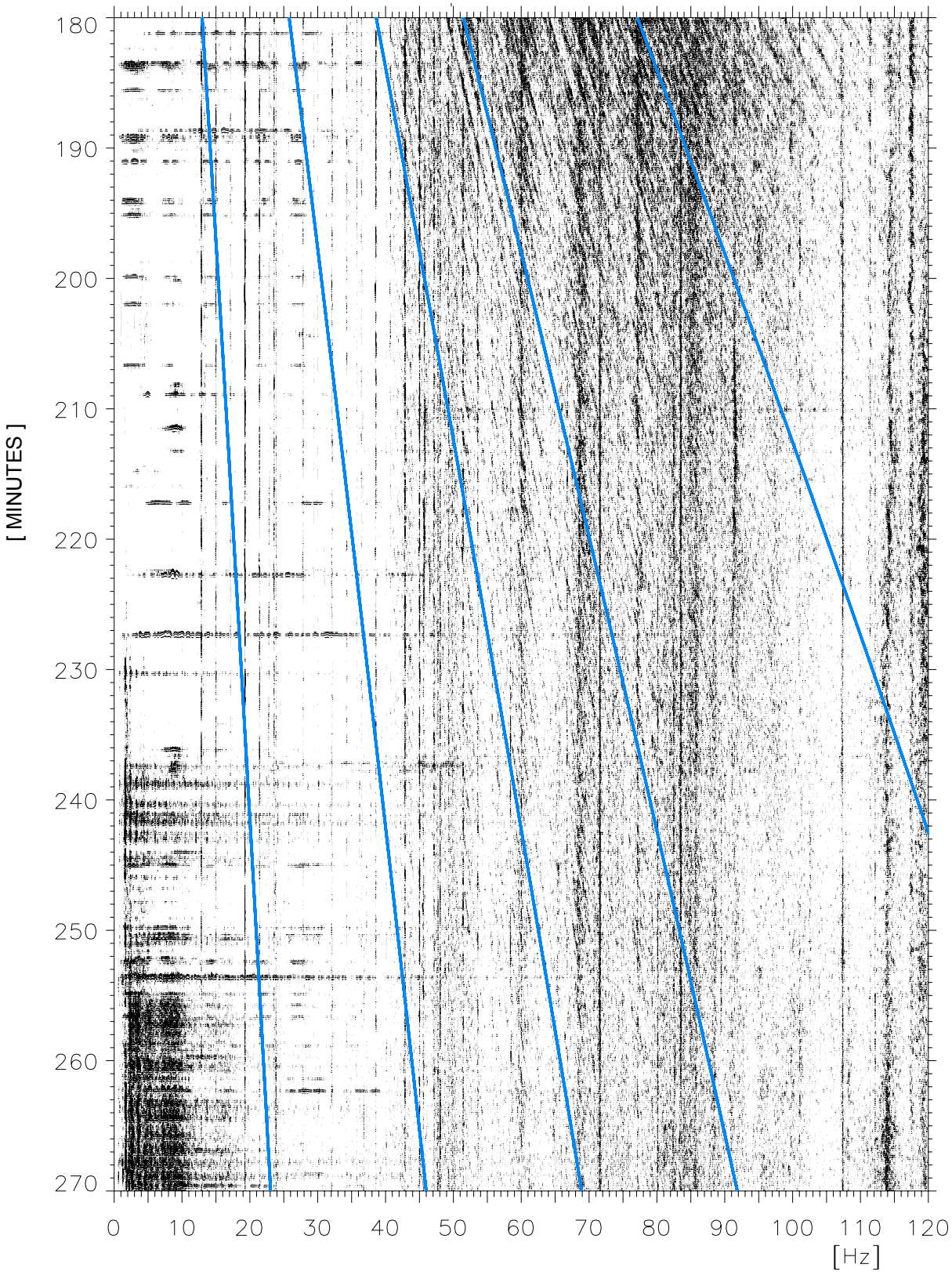

Figure 5.3 Lofargram for western run, second part. Frequency resolution 0.05 Hz. Assumed target speed 15 knots. Blue lines: striation patterns with CPA = 6 km and $\beta = 0.8$

5.5 A localization "exercise"

The theoretical striation patterns in Figures 5.1 – 5.3 seem reasonably correct when looking at the full pictures. A small analysis exercise was executed, trying to estimate ranges by means of templates for *limited* parts of the lofargrams. The conditions were as following,

(a) frequency range 40 – 90 Hz
(b) 10 minutes sections of the lofargrams at a time
(c) templates with CPA = 0 and templates with CPA = 6 km
(d) templates with $\beta = 0.8$ and templates with $\beta = 1$
(e) target always assumed approaching, also from the west

As to Item (c) and the 6 km CPA, it was in Chapter (d) estimated a CPA of 4 – 6 km. Fixing it at 6 km is a result of template adjustment. As to Item (e), the striations are expected to be almost the same for ingoing and outgoing targets.

The actual lofargrams used in the "exercise" are not shown here, but they were expanded versions of those shown above. The template comparisons were done manually, which introduces a subjective element. However, it was tried to do the comparisons as unprejudiced as possible, and as independent of each other as possible.

Figure 5.4 shows the results for the eastern part, giving as asterisks the estimated ranges versus the "true" ones. The $\pm 10\%$ error limits are indicated. The values relating to CPA = 6 km (red) and to CPA = 0 (blue), respectively, do not deviate much from each other except at close ranges. Thus the straight-line template works well outside say 10 – 15 km. That it does not do that at close ranges when only 10 minutes are observed, is natural. Such a situation is easily detectable by strongly curved striations.

Figure 5.5 shows the same for the target hypothetically approaching from the west. At the longest ranges it was not possible to make estimates over only 10 minutes; therefore the whole history "up to now" was used. At the most extreme range a β value even smaller than 0.8 might have been appropriate. At intermediate ranges $\beta = 0.8$ gave good results, at closer ranges $\beta = 1$. At close ranges the CPA = 0 km template gives some deviations.

As a general observation, the straight-line templates assuming CPA = 0 work well at long ranges, a somewhat comforting feature. However, it is important to have an approximately correct β value.

Appendix C contains a discussion of cases where the harmonics are few. The problem of then establishing the striation patterns is looked into.

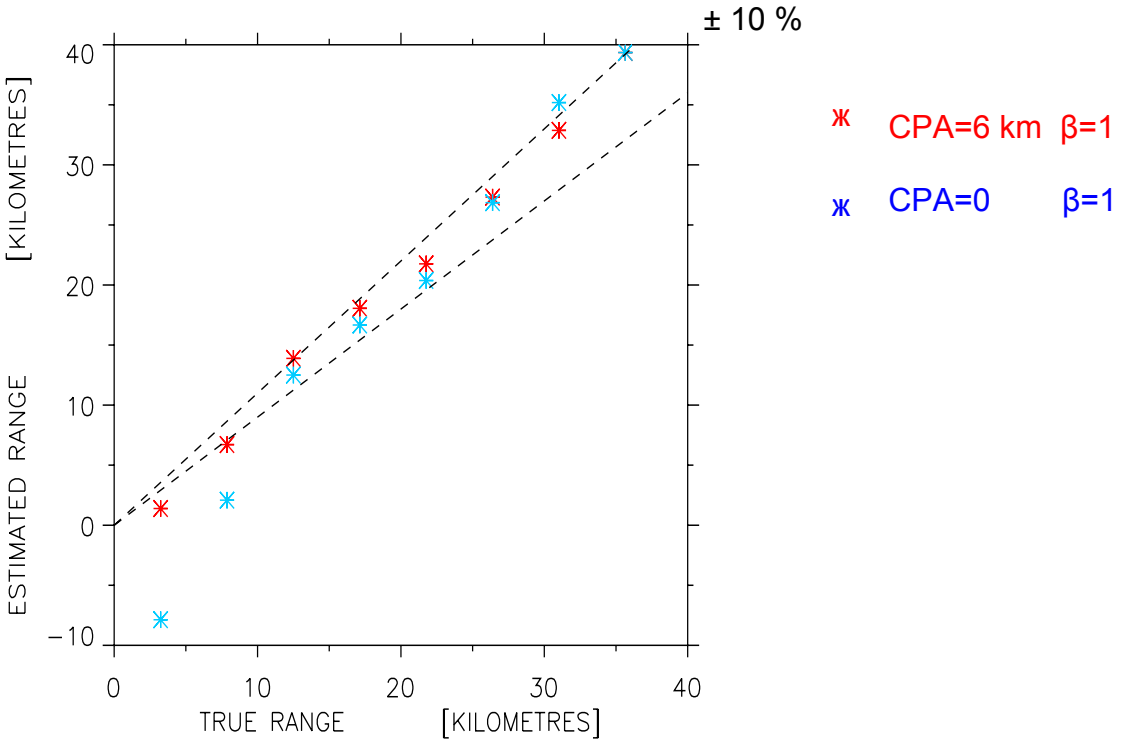

Figure 5.4 Localization results, eastern run. 10 minutes sections of lofargrams.

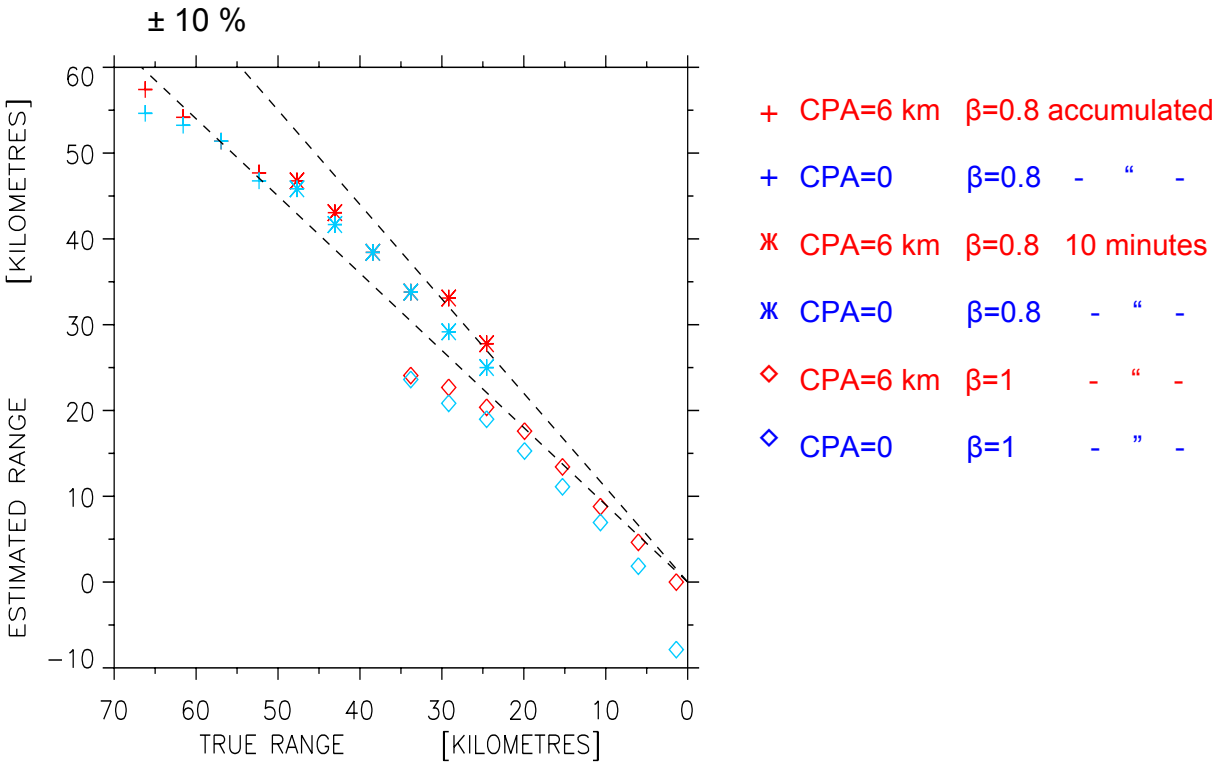

Figure 5.5 Localization results, western run

6 STRIATION SPEED

The striations can be pictured as a set of annuli that moves with the source, Figure 6.1. In a situation with varying sea depth and other propagation influences, the annuli can no longer be expected to be circular. They will change shape as the target is moving.

The striations will intersect the receiving array, and their speed along the array can be measured. This speed is of course related to the target's speed, but is also dependent upon bathymetry, orientation of the array and the track offset (CPA). Expressions relating the striation speed along the array to the target speed under these influences will now be found.

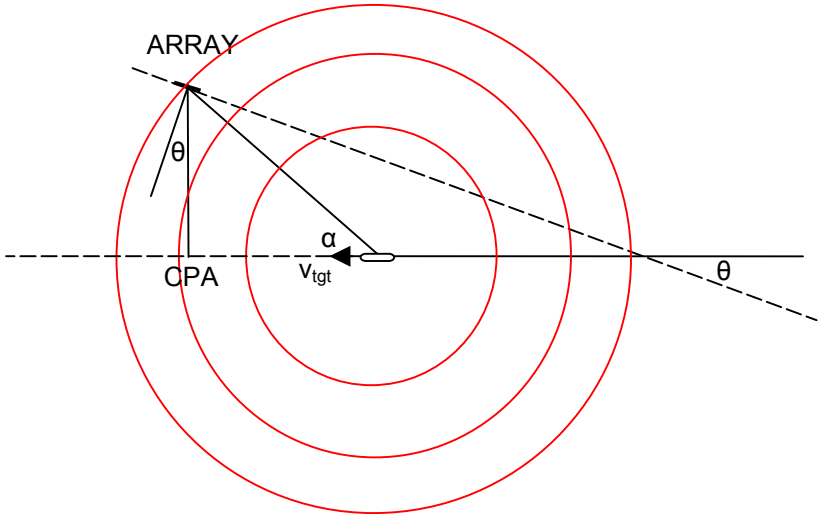

Figure 6.1 Skew target track with CPA offset. Striation annuli

6.1 Influence of target track angle and CPA offset

A skew track in combination with a CPA offset can have quite a dramatic effect. Consider a case with flat bathymetry. The striations are then circular. Figure 6.1 gives a bird's view, defining the track angle θ and the array's bearing angle α from the source. The striation annuli will move unchanged with the source at the same speed v. Figure 6.2 shows in detail a striation at the array before (blue) and after (red) the source has moved a small distance Δ. During the movement the striation will move along the array a distance Δ' that here is smaller than Δ. This means that the apparent (and measurable) striation speed at the array will be smaller than the nominal v. By simple trigonometry,

$$\Delta' \cos(\alpha - \theta) \approx \Delta \cos\alpha \qquad or \qquad \frac{v_{meas}}{v} = \frac{\Delta'}{\Delta} \approx \frac{\cos\alpha}{\cos(\alpha - \theta)} \tag{6.1}$$

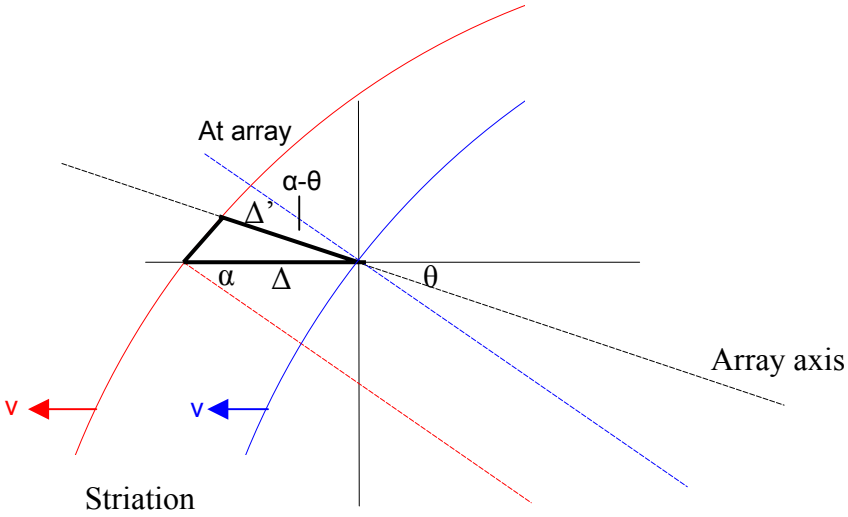

Figure 6.2 Geometry for skew array and target track offset.
Blue: source and striation before small step Δ
Red: source and striation after small step Δ

This scaling is plotted in Figure 6.3 for CPA=6 km and θ=26º. Range is measured along the target track, with zero km at the CPA point where α=90º. Broadside is α=90º+θ. For α larger than broadside the speed scaling is always higher than 1. For α less than broadside it is smaller than 1. Near the array, the measurable striation speed will be grossly blown up in magnitude. In a certain area it will even be negative. This is a peculiarity due to the skew array. The CPA offset is implicit in the angle α. The deviation of v_{meas} from the true v will be larger with increasing CPA offset. For long ranges,

$$\frac{v_{meas}}{v} \rightarrow \frac{1}{\cos\theta} \tag{6.2}$$

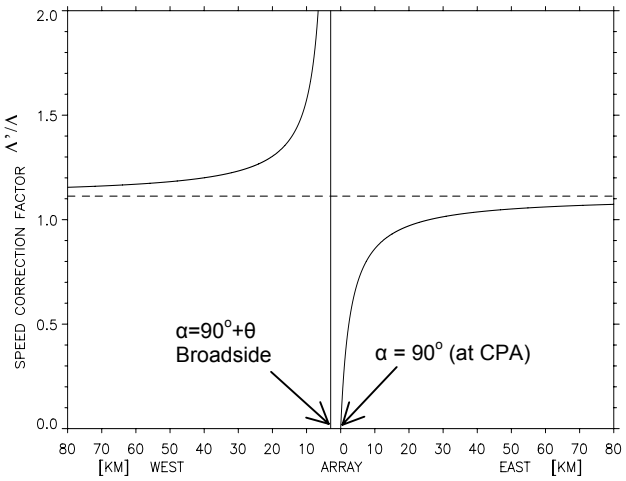

Figure 6.3 Scaled striation speed along array with skew array and track offset.

6.2 Influence of bathymetry

Assume now that the target is moving on a constant course, in-line with the receiver, which could be a single hydrophone. Consider two dominant modes, m and n. In a constant waveguide the observed striation pattern as a function of range is determined by the phase term in Equation (3.2), namely

$$phase = (k_m - k_n)\, r \tag{6.3}$$

In a situation with changing bathymetry between source and receiver but otherwise "adiabatic" conditions (no energy exchange between modes), the appropriate phase term is (6)

$$phase = \int_0^r \left[k_m(x) - k_n(x)\right] dx \tag{6.4}$$

where the wavenumbers are given by the textbook expression

$$k_m(x) = \sqrt{\left(\frac{\omega}{c}\right)^2 - \left((m - \tfrac{1}{2})\frac{\pi}{d(x)}\right)^2} \tag{6.5}$$

and d(x) is the bottom profile between source and receiver.

The relation between target speed v and striation speed v_{str} at the array will now be found. Striation is defined as a pattern having *constant* phase as time goes by, that is as the source is moving. Consider the following phase condition between the target at range r_{tgt} and a striation at range r_{str}. For constancy over time

$$\frac{d}{dt}\, phase(r_{tgt}, r_{str}) = \frac{d}{dt} \int_{r_{tgt}(t)}^{r_{str}(t)} \left[k_m(x) - k_n(x)\right] dx = 0 \tag{6.6}$$

By Leibnitz' rule this has the solution

$$\left[k_m(r_{str}) - k_n(r_{str})\right] \frac{dr_{str}}{dt} - \left[k_m(r_{tgt}) - k_n(r_{tgt})\right] \frac{dr_{tgt}}{dt} = 0 \tag{6.7}$$

Now $r_{tgt} = r$, $dr_{tgt}/dt = v$, $r_{str} = 0$ and $dr_{str}/dt = v_{str}$, giving

$$\left[k_m(0) - k_n(0)\right] v_{str} = \left[k_m(r) - k_n(r)\right] v \qquad or \qquad \frac{v_{str}}{v} = \frac{k_m(r) - k_n(r)}{k_m(0) - k_n(0)} \tag{6.8}$$

This can be simplified by using the approximation $(1-\varepsilon)^{1/2} \approx 1 - \varepsilon/2$ for small ε (which is the case here) in Equation (6.5), giving eventually

$$\frac{v_{str}}{v} \approx \left(\frac{d(0)}{d(r)} \right)^2 \tag{6.9}$$

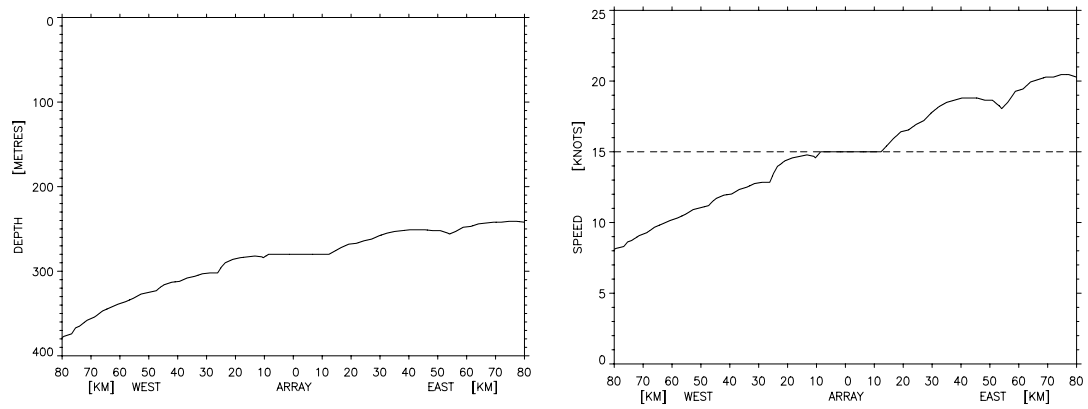

(a) (b)

Figure 6.4 (a) Approximate bathymetry for western and eastern runs
(b) Expected striation speed at the receiver as function of target range along the bathymetric profile

Figure 6.4.a shows the bathymetric profile for the combined runs. The striation speed at the array according to Equation (6.9) is drawn in Figure 6.4.b, assuming a source speed of 15 knots. Thus with increasing depth under the source, the striation speed at the receiver will become slower, and vice versa.

In combining the three factors bathymetry, course and offset, for the present purpose the functions of Figures 6.3 and 6.5 will simply be multiplied, giving

$$\frac{v_{str}}{v} = \frac{\cos\alpha}{\cos(\alpha - \theta)} \left(\frac{d(0)}{d(r)} \right)^2 \tag{6.10}$$

Multiplication seems justifiable, as the causes are different (vertical versus horizontal effects). This will be used when comparing measurements with theory in the next section.

6.3 Measurements

A way of determining the striation speed along an array is to plot the envelope of the narrowband signal as a function of time and hydrophone position. Figure 6.5.a shows an example. Time is along the vertical axis. The hydrophone position along the array is on the horizontal axis. The striation movements can be seen as skew straight-line patterns in the diagram. These are easily distinguishable to the eye. The slope of the pattern is in minutes per metres, i e the inverse of speed. The steeper the slope, the lower the speed. The slopes corresponding to 10, 15 and 20 knots are indicated.

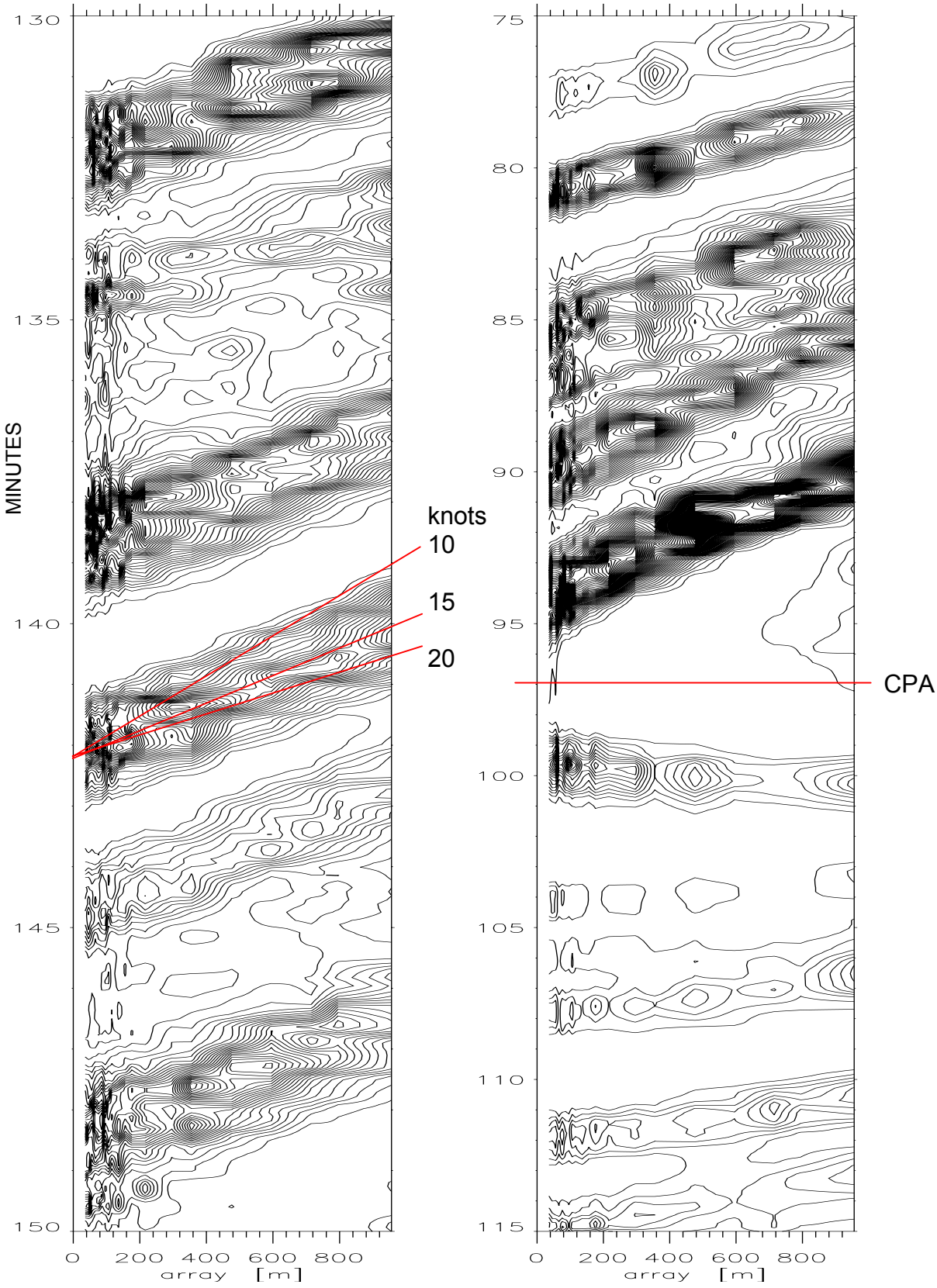

(a) Source 15 – 25 km W

(b) Source passing the CPA

Figure 6.5 Striation movement along array at 19.4 Hz.

Six of the target's harmonics have been picked for analysis, namely 12.7, 13.4, 19.4, 38.7, 44.7 and 107.7/108.5 Hz. The results are plotted in Figure 6.6. The continuous curves are the theoretical values based upon bathymetry, track skew angle = 26° and CPA = 6 km offset. The speed values were manually read off Figure 6.5.a type diagrams by means of a template.

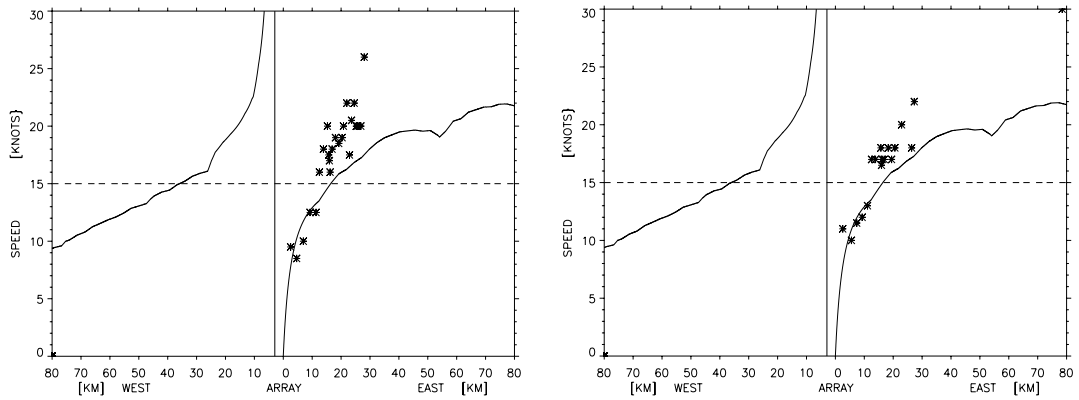

(a) 12.7 Hz (b) 13.4 Hz

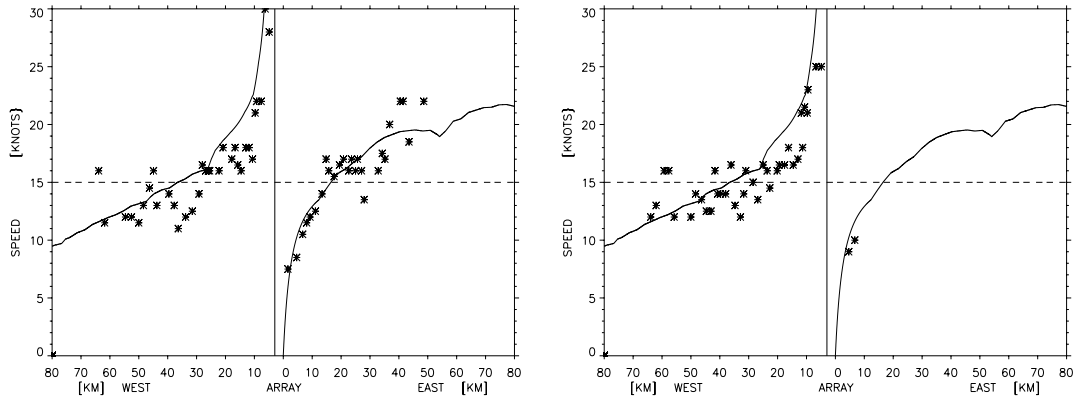

(c) 19.4 Hz (d) 38.7 Hz

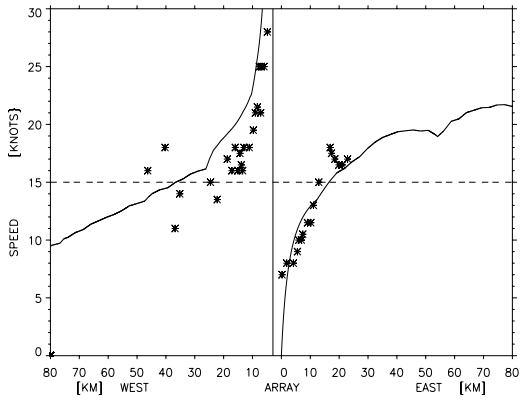

(e) 107.7 Hz (left) 108.5 Hz (right)

Figure 6.6 Measured striation speed along array compared to theoretical predictions
Continuous lines: theory Asterisks: measurements

The measured data follow mostly the trends in the theoretical values. At the two lowest frequencies there is some mismatch. It should be pointed out that the bathymetries used here are not exactly those relating to the tanker situation, but are taken from the auxiliary runs, as shown in Figure 1.1. There could also be other environmental influences. The spread in the data can partly be due to the rather coarse way of estimating slopes from diagrams like Figure 6.5.a. However, the theory seems to encompass the important effects. Figure 6.5.b gives an example of what happens when the source is close to the array. The slopes behave qualitatively as theoretically predicted. Even a negative speed can be seen.

Thus the striation speed as measured on an array is fairly sensitive to the geometry of track versus array, but mathematically predictable. This sensitivity could be of advantage in certain applications. But it also means that to observe a *single* striation passage over the array will hardly be enough. One would need observations over time, possibly together with other inputs (such as bearing).

At close ranges there will be near-field effects, indicated by the curved patterns in Figure 6.5.b. The determination of speed over the array was also attempted done in quite a different way, namely in analogy with beamforming. The hydrophone signal envelopes were lined up and summed at trial speeds. This gave no success. The direct way of Figure 6.5 was the best for visual detection of striation passages, due to the eye's pattern recognizing capability.

In Appendix D similar results for a 40 Hz towed source are given.

7 SPEED BY DOPPLER AND ANGLE OF MODES

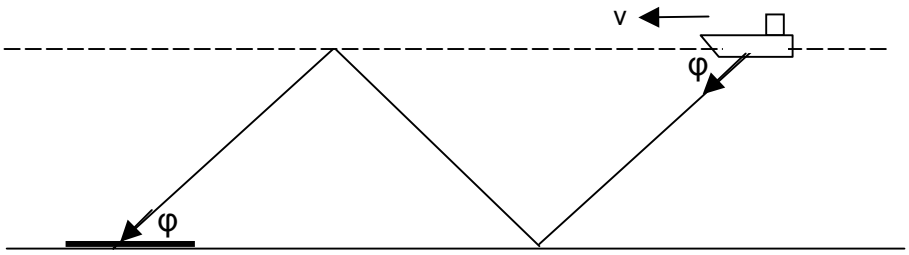

Figure 7.1 Grazing angle of a mode in an ideal waveguide. Doppler component is v cosφ

This method is based upon an earlier concept, demonstrated on data from CW-towings in Vestfjorden in 1986-87 (7), (8). The idea is to resolve the received mode signals simultaneously in doppler frequency and vertical angle, and read off a certain slope in that 2-dimensional representation. In Figure 7.1 a ray (mode) is illustrated. It has a grazing angle φ with the horizontal. The doppler shift of the signal is determined by the source speed component in the φ direction,

$$\Delta f = \frac{v}{c} f_0 \cos\varphi \tag{7.1}$$

The lowest order modes, which are closest to horizontal propagation, will have maximum doppler shifts. The higher order modes will have increasingly smaller shifts. Thus in a reasonably ideal waveguide there is a linear relationship between doppler shift and cosine of grazing angle. This means that in a frequency versus cosφ diagram the intensities will lie as maxima on a straight line. Figure 7.2 gives examples of such 2D presentations, taken from the tanker data.

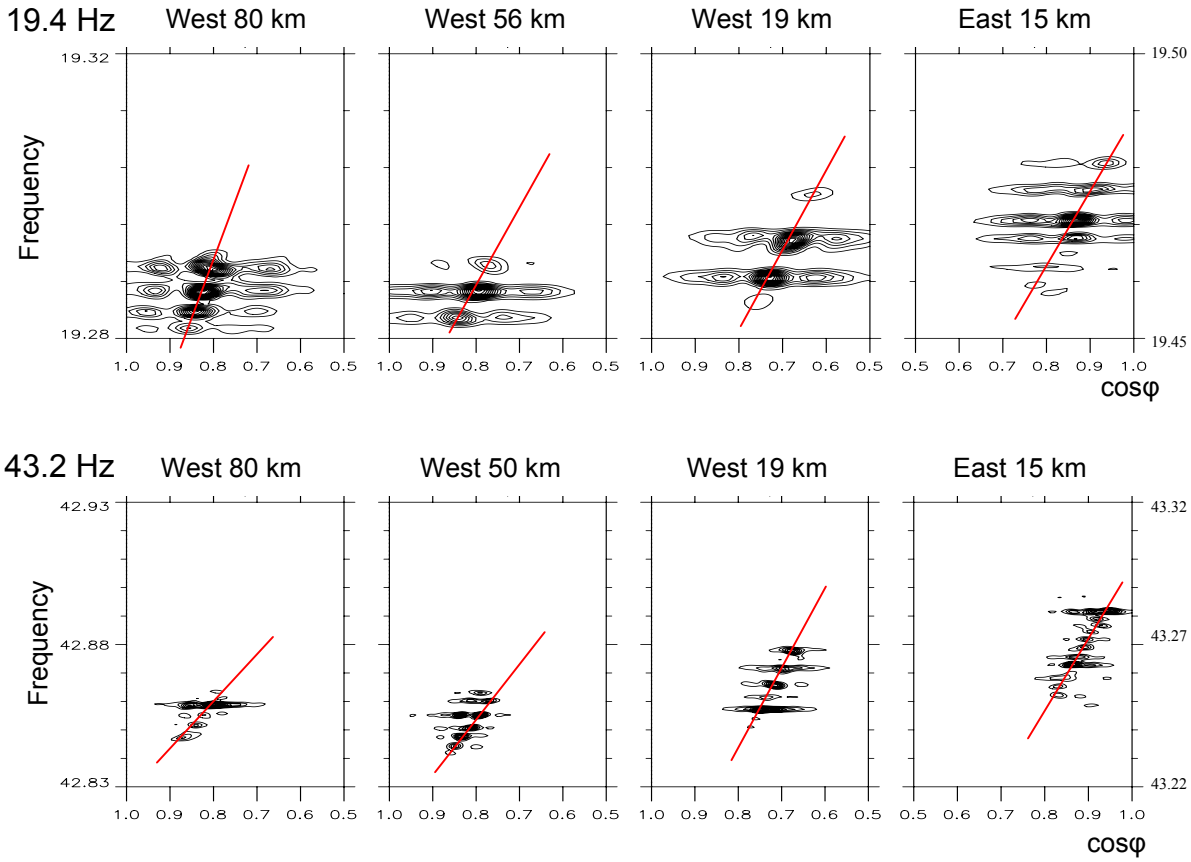

Figure 7.2 Doppler frequency versus cosine of grazing angle for 19.4 and 43.2 Hz
West: negative doppler East: positive doppler

If the slope (red line) is extended until it crosses the cos0°=1 and the cos90°=0 axes, then using Equation (7.1)

$$slope = \frac{d(\Delta f)}{d(\cos\varphi)} = \frac{v}{c} f_0 \tag{7.2}$$

This gives a measured speed of

$$v_{meas} = \frac{c}{f_0} slope \tag{7.3}$$

It is not necessary to determine f_0 accurately, the received frequency can be used instead,

$$v_{meas} = \frac{c}{f_{meas}} slope \tag{7.4}$$

This gives only a small error (0.5% at 15 knots). The slope can be read off manually or electronically by using templates with trial slopes for different v. The above applies to a flat waveguide and an endfire source. Two extended cases will now be considered: off-endfire track with offset, and varying bathymetry.

7.1 Influence of track angle and CPA offset

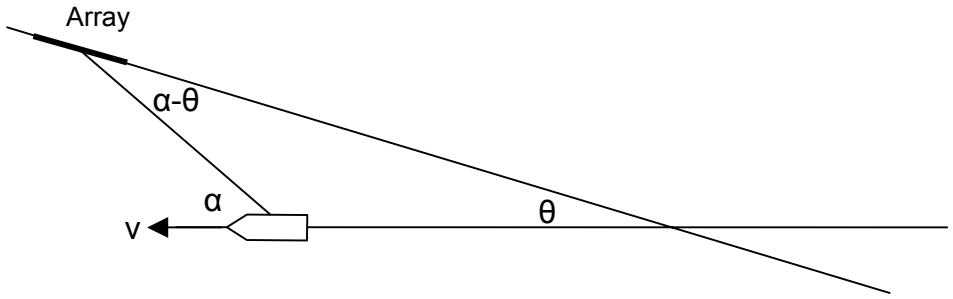

Figure 7.3 Skew track with CPA offset. Definition of angles

In Figure 7.3 the angle α is the horizontal bearing angle of the array from the source. Doppler shift is determined by the speed component in that direction together with the grazing angle φ,

$$\Delta f = \frac{v}{c} f_0 \cos\varphi \cos\alpha \tag{7.5}$$

The horizontal direction of the source *from* array endfire is α-θ, the vertical direction is φ. The resulting angle φ' measured from the array endfire will then be given by

$$\cos\varphi' = \cos\varphi \cos(\alpha - \theta) \tag{7.6}$$

The *slope* of the patterns can now be found by using the grazing angle limits φ=0° and φ=90° giving

$$slope = \frac{d(\Delta f)}{d(\cos\varphi')} = \frac{v}{c} f_0 \frac{\cos\alpha}{\cos(\alpha - \theta)} \tag{7.7}$$

Using the same templates as above, there will be a correction term to v, such that v_{meas} is given by

$$v_{meas} = \frac{c}{f_0} slope = v \frac{\cos\alpha}{\cos(\alpha - \theta)} \tag{7.8}$$

This function is shown in Figure 7.4, giving the measured speed along the array as function of range. The speed v along the target's track is set to 15 knots. The values vary dramatically close to the array, due to the combination of the skewness and the offset of the track. This is in fact the same function that was found in Chapter 6 (Figure 6.3) for a different measurable quantity.

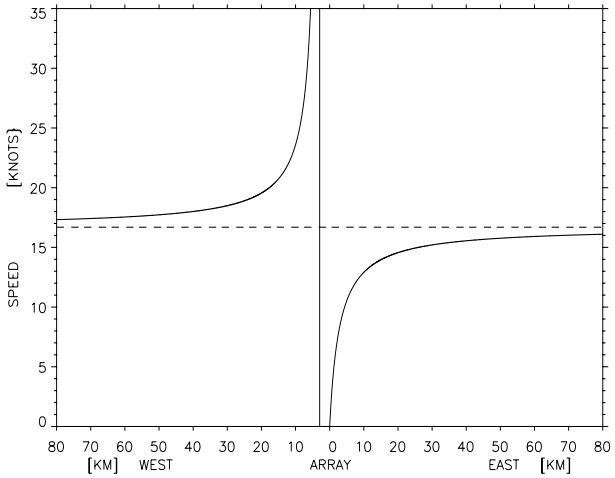

Figure 7.4 Theoretical values for speed by the slope method with skew track and CPA offset

7.2 Influence of bathymetry

Figure 7.5 shows a case with varying depth, and indicates that the grazing angle φ'' as measured at the array will be smaller than the angle φ at the source for downhill propagation, and vice versa.

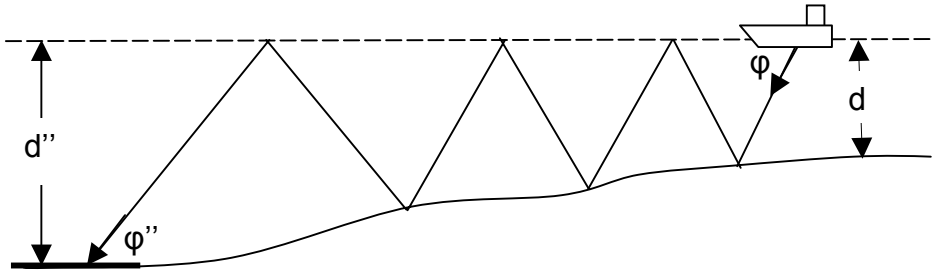

Figure 7.5 Grazing angle of a mode with downhill propagation

The textbook expression for the grazing angle of a mode in an ideal waveguide is

$$\sin\varphi = \left(n - \tfrac{1}{2}\right)\frac{\pi}{d}\frac{c}{\omega} \tag{7.9}$$

where d = sea depth. Assuming "adiabatic" conditions (the mode keeps its integrity) (6) for a non-flat waveguide, and using the expression above,

$$\frac{\sin\varphi''}{\sin\varphi} = \frac{d}{d''} \qquad \text{and} \qquad \cos\varphi'' = \sqrt{1-\left(\frac{d}{d''}\sin\varphi\right)^2} \tag{7.10}$$

where d and d'' are the sea depths at the source and the receiver, respectively. Depth change will not affect the doppler, thus Equation (7.1) applies. The frequency versus cosφ'' slope will be

$$slope = \frac{d(\Delta f)}{d(\cos\varphi'')} = \frac{d(\Delta f)/d\varphi}{d(\cos\varphi'')/d\varphi} = \frac{v}{c} f_0 \left(\frac{d''}{d}\right)^2 \frac{\sqrt{1-\left(\frac{d}{d''}\sin\varphi\right)^2}}{\cos\varphi} \tag{7.11}$$

Using the same templates as earlier, there will be a correction term to v, such that v_{meas} is given by

$$v_{meas} = \frac{c}{f_0} slope = v\left(\frac{d}{d''}\right)^2 \frac{\cos\varphi}{\sqrt{1-\left(\frac{d}{d''}\sin\varphi\right)^2}} \tag{7.12}$$

In this case the slope is not constant. However, the middle term $(d/d'')^2$ is dominating, and the right term is fairly constant for large values of cosφ. According to Figure 7.2, cosφ = 0.8 is a typical value, which then is used all over. The function is shown in Figure 7.6, assuming v=15 knots. This is slightly different from the earlier Figure 6.5, which had $(d/d'')^2$ only.

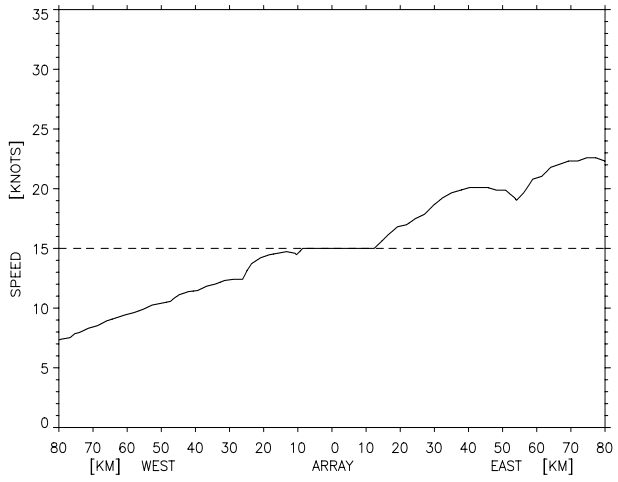

Figure 7.6 Theoretical speed by the slope method under varying bathymetry

When both skew track and varying depth are taken into account, the functions of Equations (7.8) and (7.11) are multiplied, resulting in the function

$$v_{meas} = \frac{c}{f_0} slope = v\frac{\cos\alpha}{\cos(\alpha-\theta)}\left(\frac{d}{d''}\right)^2 \frac{\cos\varphi}{\sqrt{1-\left(\frac{d}{d''}\sin\varphi\right)^2}} \tag{7.13}$$

This is being used in the next section.

7.3 Measurements

Measured speeds at 19.4 Hz and 43.2 Hz according to the "slope method" are shown in Figure 7.7, based upon signatures of the Figure 7.2 type. The readings are sometimes sparce, because a straight-line pattern could not always be established. This is especially the case for the eastern run, where the signatures are particularly difficult. A reason is possibly the special sound velocity profile (Appendix B).

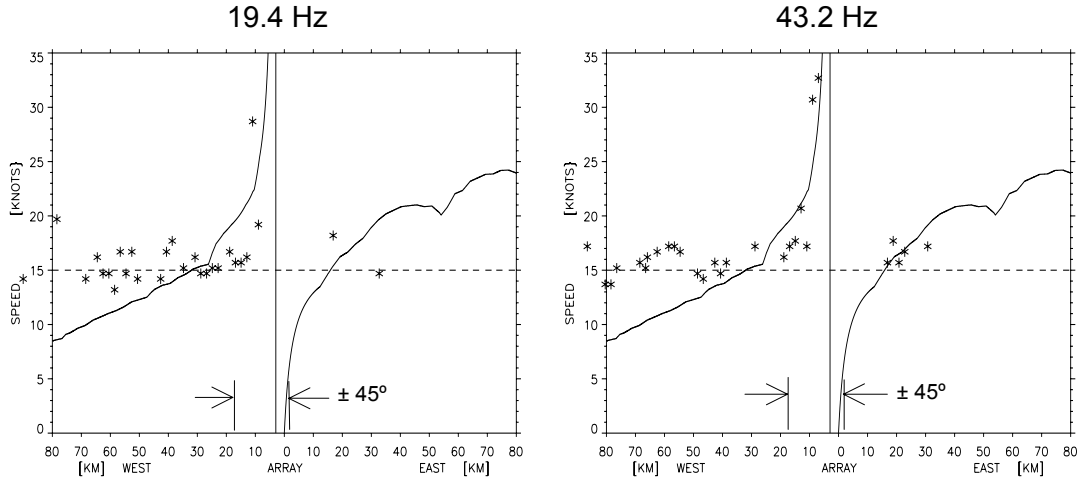

Figure 7.7 Measured speeds by the slope method
Continuous lines: theory Asterisks: measurements
± 45° around broadside array is indicated

West of 40 km the correspondence is not good. The reason is not clear. Near the array near-field effects such as uneven doppler along the array, target travel time during the integration (here 8.6 minutes), decreased array resolution for vertical arrivals come into play. The part of the track where the source is within ±45° of broadside is indicated in the Figure.

Similar results for a towed 40 Hz source are given in Appendix D.

*

8 CONCLUSIONS

From target to acoustics. The present report is initially concerned with the so-called forward problem, namely

Given the target and its movements, together with the channel characteristics, determine the acoustics at the receiver. This is being applied to

- Determination of striation patterns as functions of frequency, range and time
- Determination of striation speed along an array
- Determination of speed from mode dopplers and angles

Confirmation. Acoustic measurements from the 2003 experiment to a large degree confirm the theoretical predictions. In particular, the striations seem to be well determined, using the waveguide invariant β. The speed predictions by striations seem to be well stated, also when it comes to varying bathymetry, skew track and CPA offset. The mode approach was less successful.

From acoustics to source localization. This so-called inverse problem,

Given the acoustic measurements, determine the target's movements

is also being addressed, but to a less degree. A small localization "exercise", based upon striations only, was reasonably successful.

In a wider context, target localization could be done using all available and relevant acoustical information, such as

- high resolution bearing changes
- high resolution doppler changes
- striation patterns

These could be input to a track estimator. The acoustical information considered in this report is all produced by use of conventional signal and array processing techniques. Modelling the transmission channel as such is not done. Instead the channel characteristics are lumped into the waveguide invariant β. This restricts the applicability to waveguides of somewhat idealised behaviour. Gently varying bathymetry is allowed, though.

References

(1) Chuprov S D (1982): Inteferentsionnaya struktura zvukovogo polya v sloistom okeane (Interference structure of a sound field in a layered ocean), in Akustika Okeana. Sovremennoe sostoyanie (Ocean Acoustics. Current state), ed by L M Brekovskikh, I B Andreevoi, Nauka, Moscow 1982, pp 71-91 (In Russian)

(2) D'Spain G L, Kuperman W A (1999): Application of waveguide invariants to analysis of spectrograms from shallow water environments that vary in range and azimuth, J Acoust Soc Am 106 (5), November 1999, pp 2454-2468

(3) Yang T C (2003): Beam intensity striations and applications, J Acoust Soc Am 113 (3), march 2003, pp 1342-1352

(4) Heaney K D (2004): Rapid geoacoustic characterization using a surface ship of opportunity, IEEE J of Oceanic Eng, vol 29, no 1, January 2004

(5) Tollefsen D, Eidem E J, Svolsbru T, Torgersen T (2003): Project SWASI III: Technical cruise report from Phase S-iiib 2003 – The SWASI-03 array experiment, FFI/RAPPORT-2003/03005, Exempt from public disclosure

(6) Zakarauskas P, Dosso S E, Fawcett J A (1996): Matched-field inversion for source location and optimal equivalent bathymetry, J Acoust Soc Am 100 (3), September 1996, pp 1493-1500

(7) Søstrand K A (1990): The "Vær" experiment – mode filtering in the doppler frequency and horizontal wavenumber domains – Vestfjorden September 1986 and May 1987, FFI/RAPPORT-90/2002, Restricted

(8) Glattetre J, Knudsen T, Søstrand K (1989): Mode interference and mode filtering in shallow water: A comparison of acoustic measurements and modelling, J Acoust Soc Am 86 (2), August 1989, pp 680-690

(9) Søstrand, K A (2002): Range localization of 10-100 km shots by means of an endfire array and a waveguide invariant, FFI/RAPPORT-2002/04849

APPENDICES

A TARGET SIGNATURE IN DETAIL

Figures A.1-A.6 are blown-up sections of Figure 2.1, called Vernier lofargrams. Each has a frequency span of 30 Hz. Harmonics belonging to $f_0 = 2.15$ Hz are easily identified. Namely, at the CPA-time there are slight doppler downshifts of the lines, most noticeable at the higher frequencies. By means of this doppler shift, the lines that do not belong to the target can be sorted out, if necessary by using even narrower Vernier bands. Such other lines can be seen for instance at 35.7 Hz, 89.5 Hz and 107.3 Hz.

The set of harmonics of $f_0 = 2.15$ Hz corresponds to a propeller shaft rate of RPM = 129. The lines are sharp, and are probably caused mostly by the main machinery radiating via the hull, not via the propeller. The harmonic set has no evident modulation from a certain number of propeller blades. This supports the assumption about hull radiation. Nor is there any evident modulation from a number of cylinders. The frequency width of the harmonics increase with increasing frequency, as can be expected.

There are some lines with doppler shift at the CPA-time that are not related to f_0. Such can be seen at 29.5 Hz and 177-8 Hz . Auxiliary machinery must be the sources. The two lines at 116 and 118 Hz are very strong compared to the other lines. One or both could therefore be caused by auxiliary machinery, possibly masking underlying harmonics.

In between the harmonic lines the striation patterns are strong. This indicates the presence of broadband noise from the ship. Both the frequency lines and the broadband noise are subject to these interferences, following the same patterns. Above 180 Hz there is still target noise, mainly broadband, but also a couple of harmonics near 180 Hz and 240 Hz (not shown in the Figures).

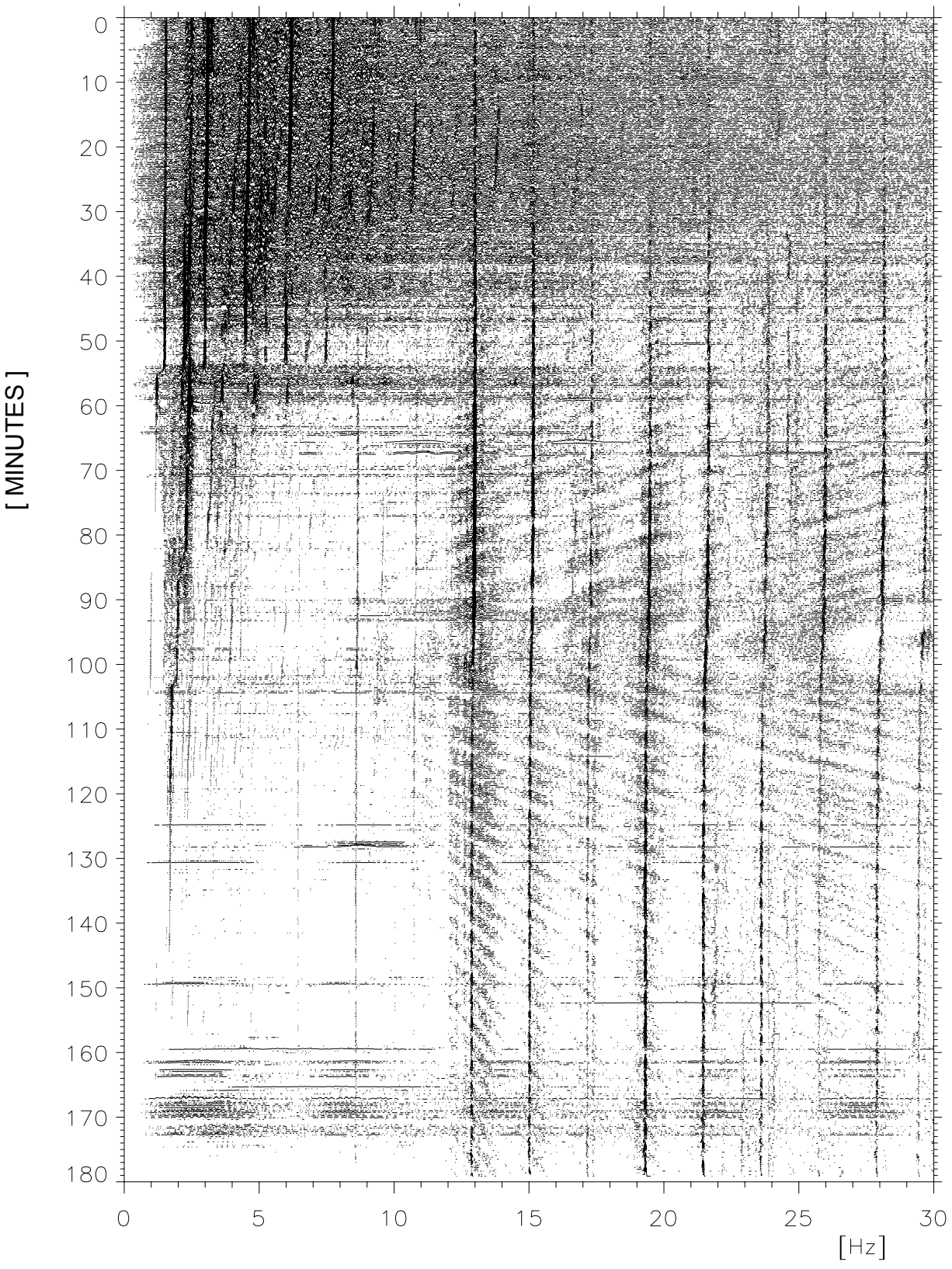

Figure A.1 Vernier lofargram for tanker, 0 – 30 Hz
Frequency resolution 0.05 Hz

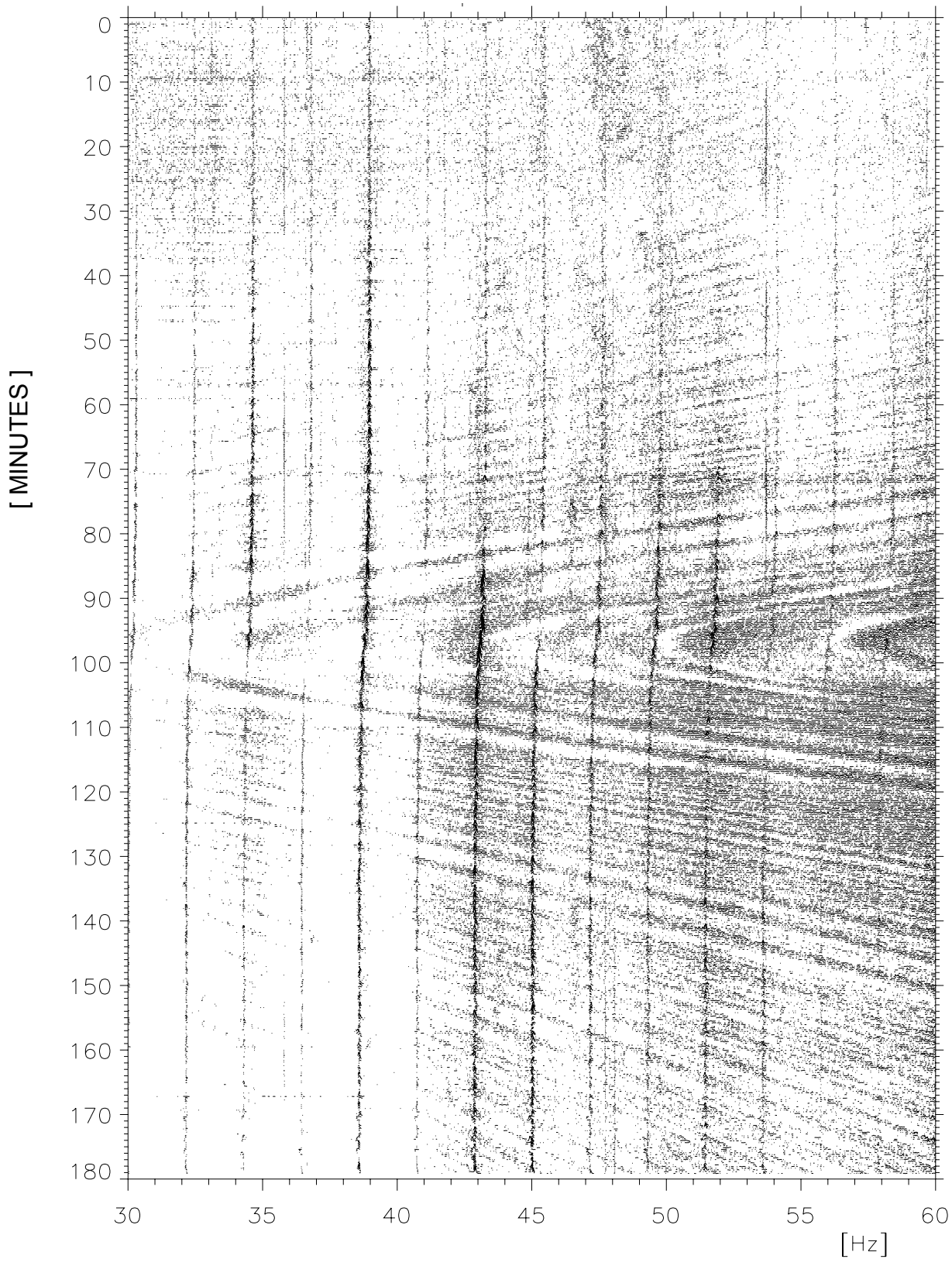

Figure A.2 Vernier lofargram for tanker, 30 – 60 Hz
Frequency resolution 0.05 Hz

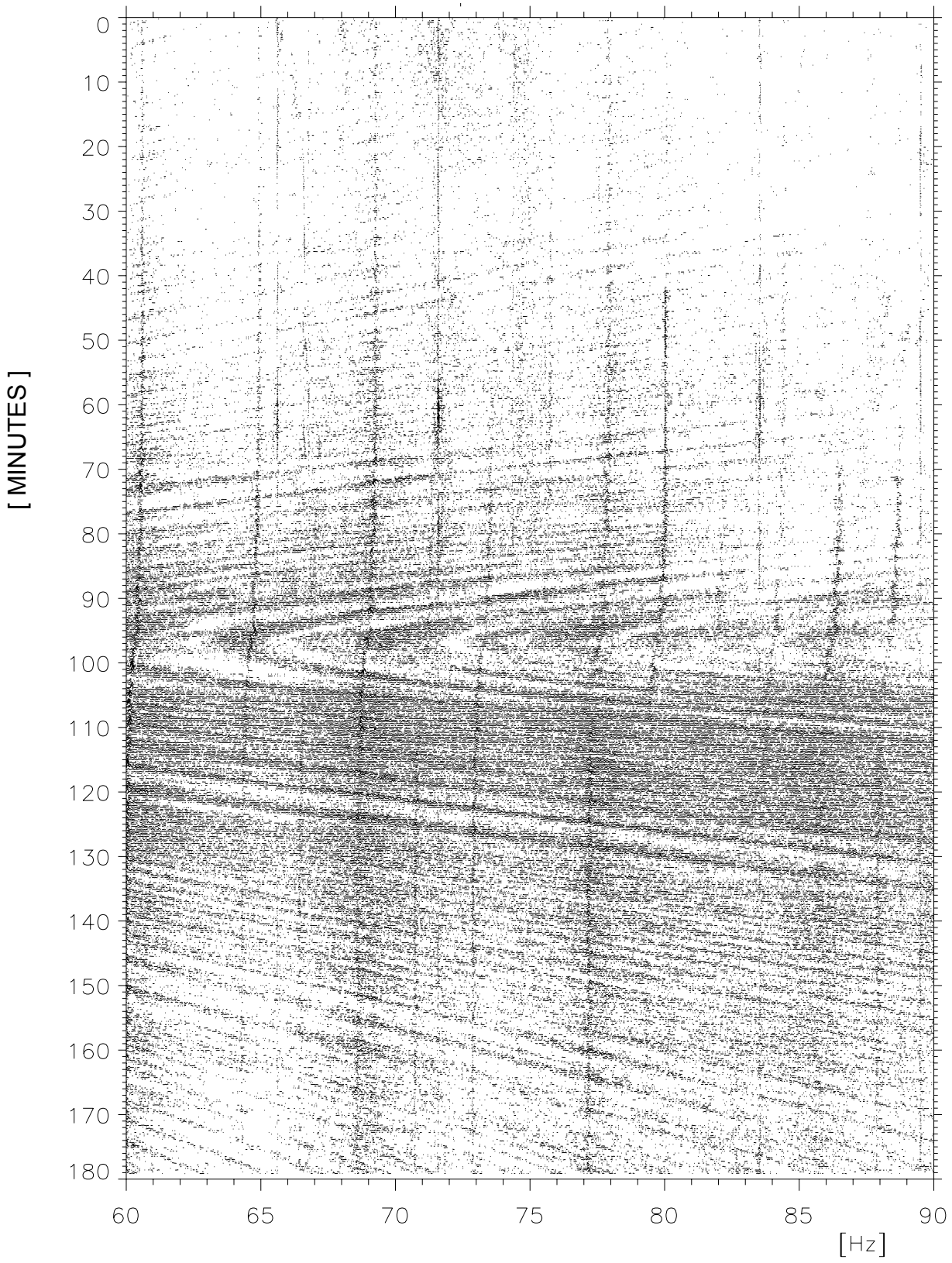

Figure A.3 Vernier lofargram for tanker, 60 – 90 Hz
Frequency resolution 0.05 Hz

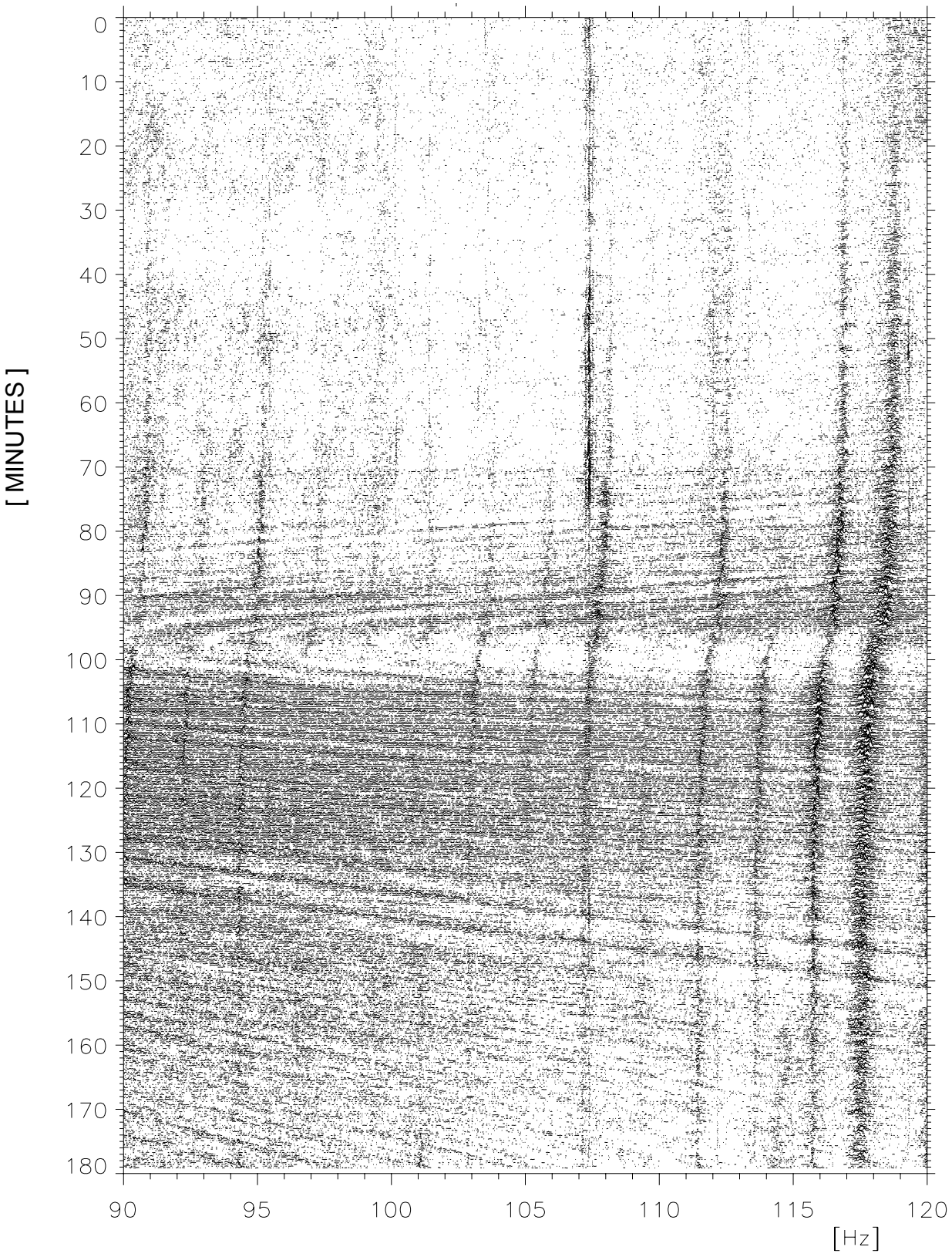

Figure A.4 Vernier lofargram for tanker, 90 – 120 Hz
Frequency resolution 0.05 Hz

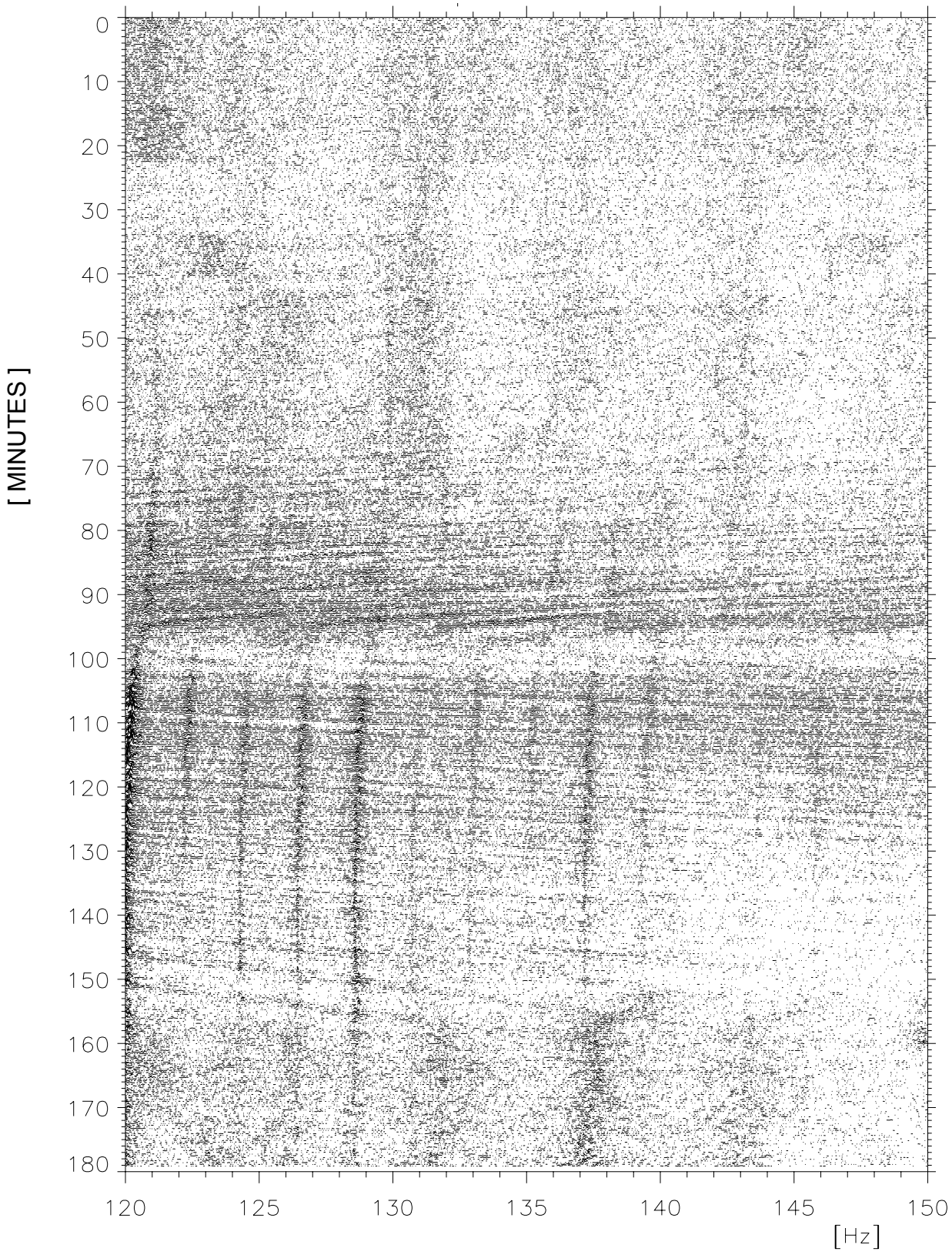

Figure A.5 Vernier lofargram for tanker, 120 – 150 Hz
Frequency resolution 0.05 Hz

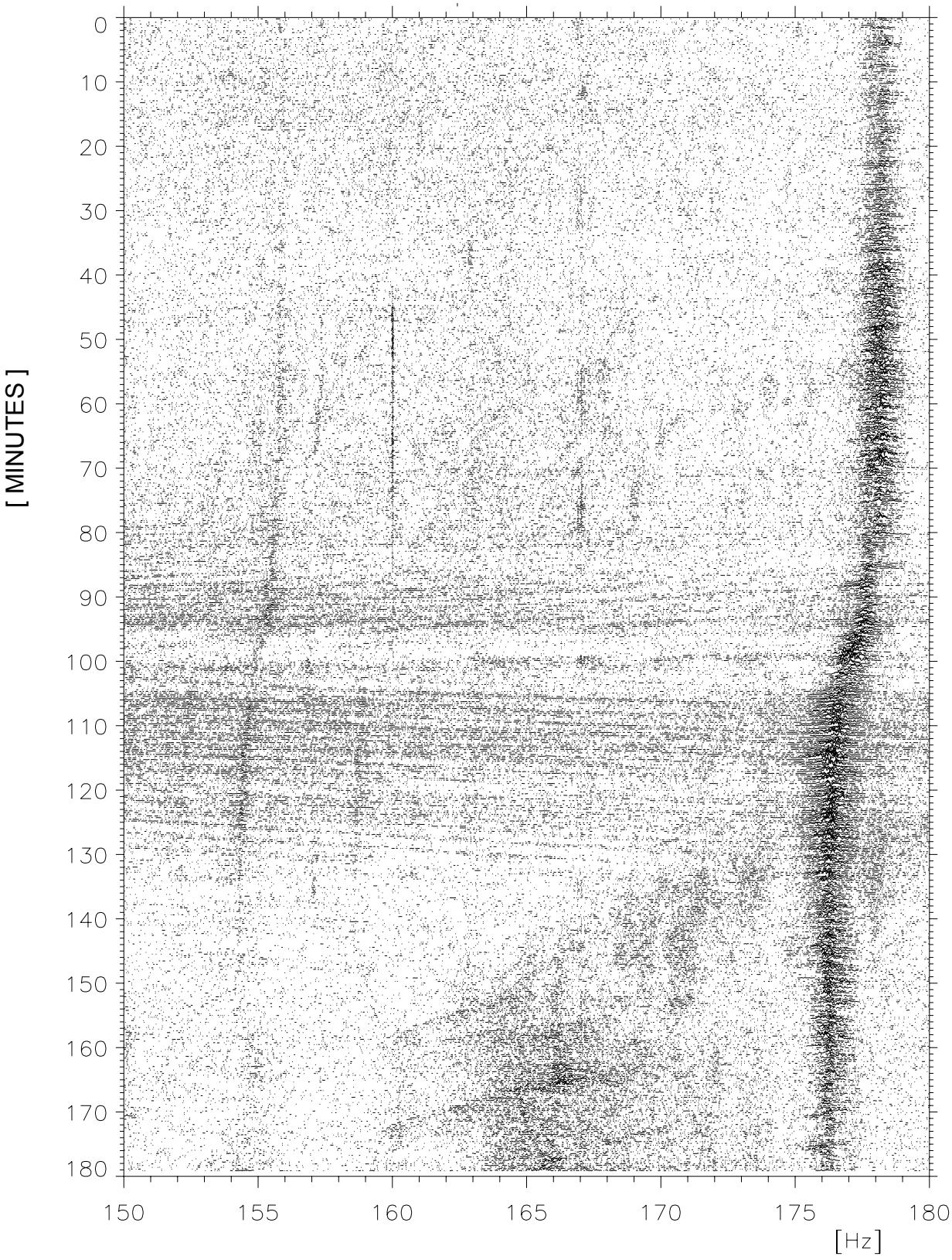

Figure A.6 Vernier lofargram for tanker, 150 – 180 Hz
Frequency resolution 0.05 Hz

B BETA FROM SUS CHARGES

As part of the experiment, two runs with SUS charges, one in the eastern and one in the western direction were made, Figure 1.1. This is similar to what was done in an experiment in 1999 at a site further north (9). The bathymetry in that area was varying, although gently. A certain success was obtained in estimating shot ranges from the received signals by using the β techniques. Range estimates were obtained by using Equation (6.1) from (9)

$$R = -\beta_{theo}\, c \;\; slope \tag{B.1}$$

where *slope* is read off a beam-time diagram for the received shot. A theoretical β_{theo} is determined from the bathymetry by the formula (2)

$$\beta_{theo}(R) \approx \left[d^2(0) \frac{1}{R} \int_0^R \frac{dx}{d^2(x)} \right]^{-1} \tag{B.2}$$

where d(0) is the depth at the receiver. This expression applies to an "adiabatic" waveguide (6). As the true ranges R_0 are known from navigation, a measured β_{meas} can be defined in analogy with Equation (B.1) by

$$R_0 = -\beta_{meas}\, c \;\; slope \tag{B.3}$$

Then

$$\frac{R}{R_0} = \frac{\beta_{theo}}{\beta_{meas}} \tag{B.4}$$

Figure B.1 shows a time-frequency diagram for a shot arrived from 66 km west. The frequency resolution is 1/12 octave. The patterns reflect the modes.

Figure B.2 shows how the slopes are defined. Outputs from the beamformer at four different frequencies in beam-time diagrams are given, with (vertical) direction as cosine of angle from endfire. Mode "pulses" are quite evident. The red lines are the slopes referred to in the equations above.

Figure B.3 gives the results from the eastern run. The bathymetry is shown in the upper left diagram. In the other diagrams the continuous line is β_{theo} and the asterisks are β_{meas}. The diagrams refer to 1/3 octave bands around 32, 63 and 125 Hz. Shots inside 10-15 km are excluded, because the modes here do not resolve well in time. It can be seen that in general the measured values follow the theoretical ones. The consistency over frequency is evident. The estimation error for range can be determined by use of Equation (B.4). Typical accuracy is ±15%.

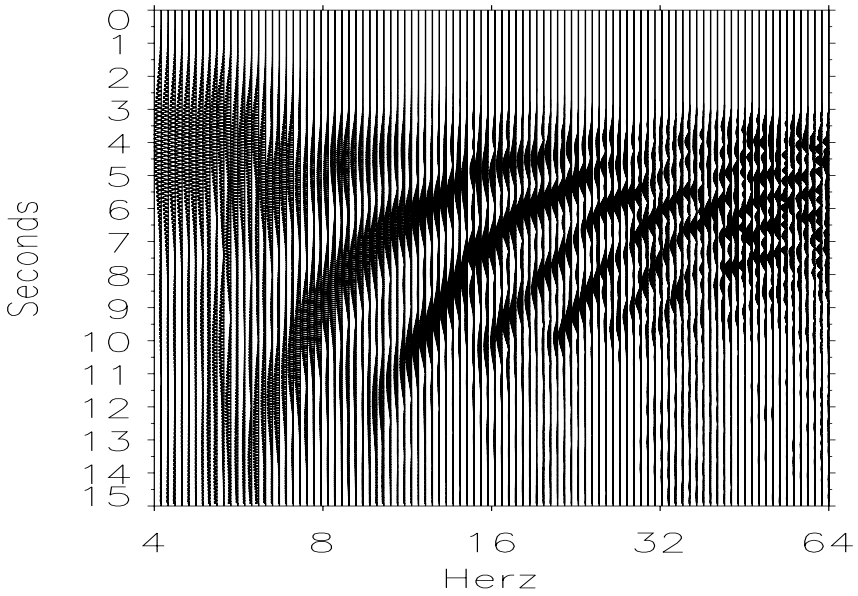

Figure B.1 Frequency-time diagram for shot from 66 km west

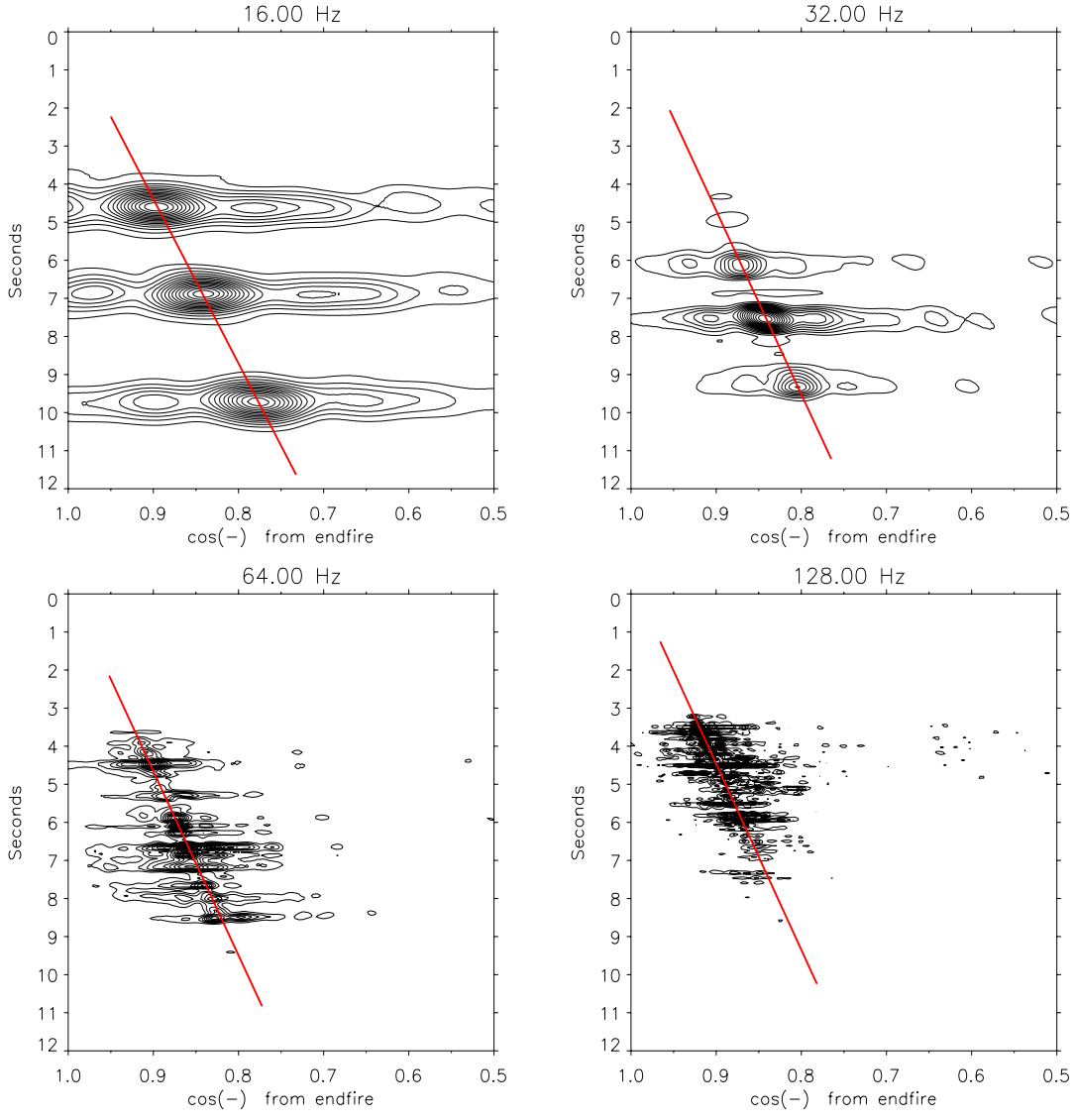

Figure B.2 Received shot signal resolved in time and vertical angle
Definition of slope

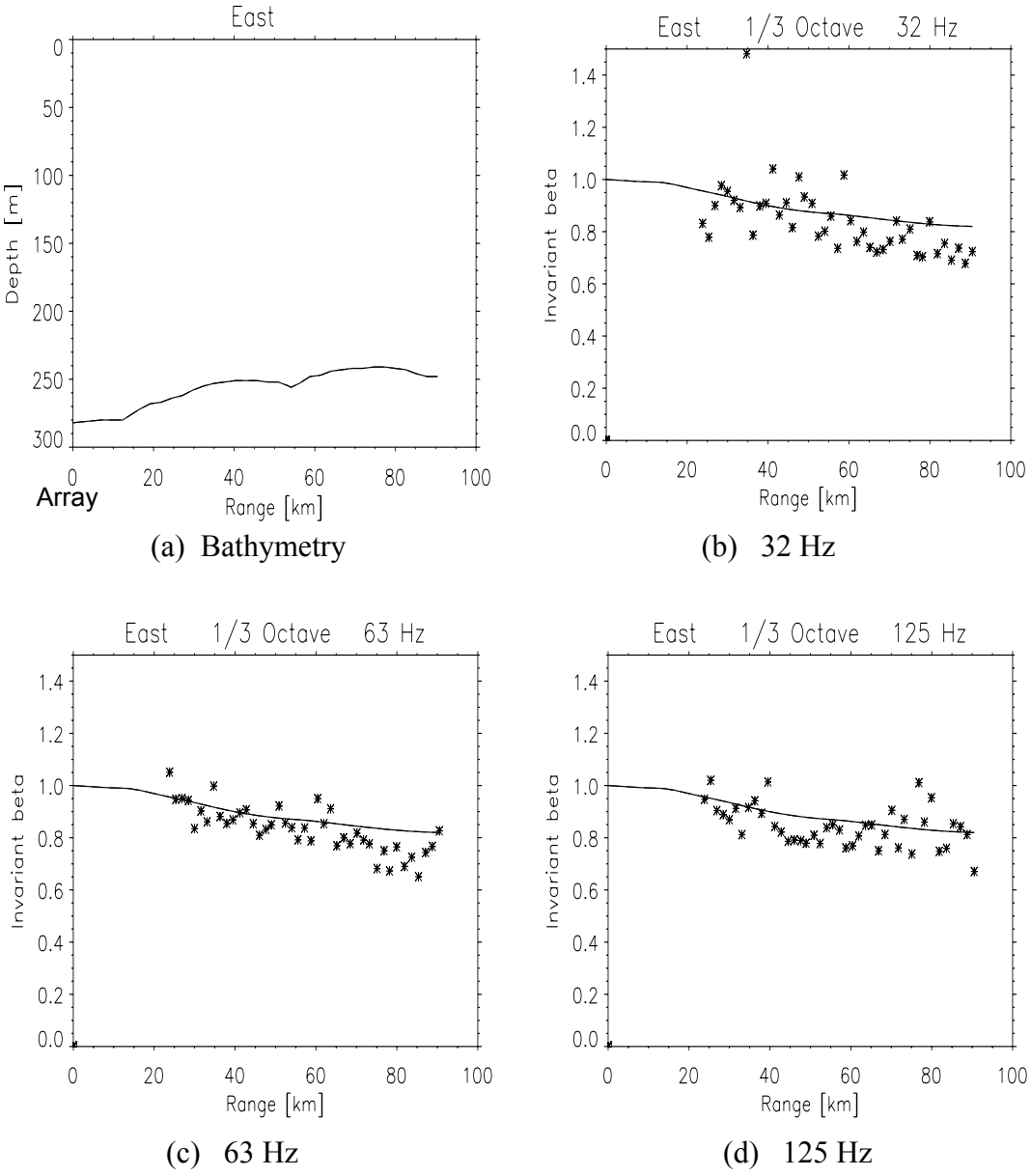

(a) Bathymetry (b) 32 Hz

(c) 63 Hz (d) 125 Hz

Figure B.3 Eastern SUS run.
(a) Bathymetry (b) - (d) Invariant β as function of range
Curve: β_{theo} from bathymetry
Asterisks: measured β_{meas}

Figure B.4 shows the same for the western run. The slope for β_{meas} has been corrected for the skew off-endfire angle (Figure 1.1). Here there is some discrepancy between theoretical and measured β values outside 40 km. Then some assumption about the ideality of the waveguide has probably been violated. This could be the presence of refracted modes. A clue is the following. Sound velocity profiles taken during the experiment are shown in Figure B.5. They indicate the presence of an internal sound channel in the water. This has the effect that when the sea depth drops below a certain value, some sound can propagate within the channel without bottom reflections. From the literature it is known that in certain channels β in fact can become negative. In the present case there probably is a mixture of bottom reflected sound and refracted sound. This makes the waveguide non-ideal, and would have a disturbing effect upon the resulting β. A conjecture is that the real β would be reduced as compared to the ideal case.

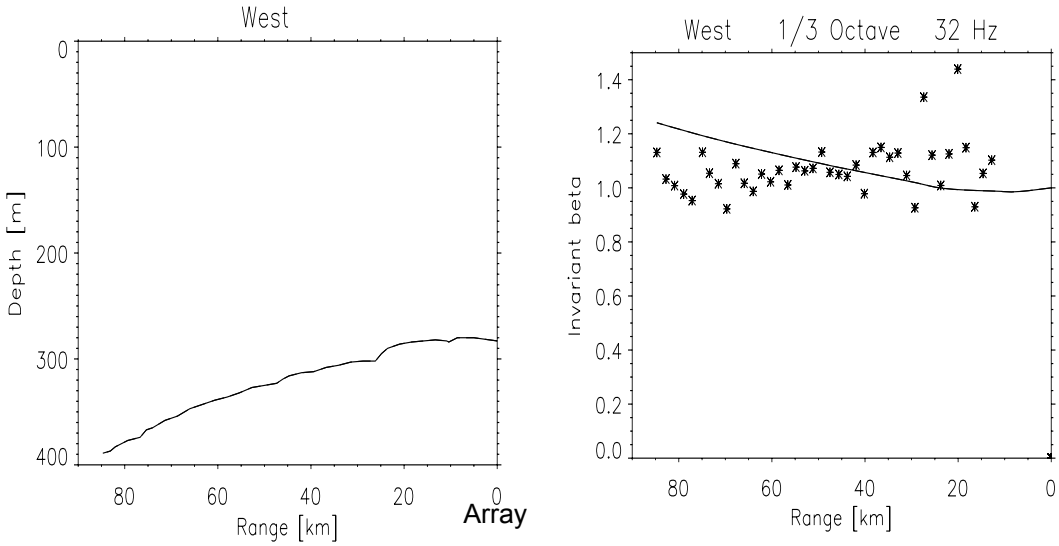

(a) Bathymetry (b) 32 Hz

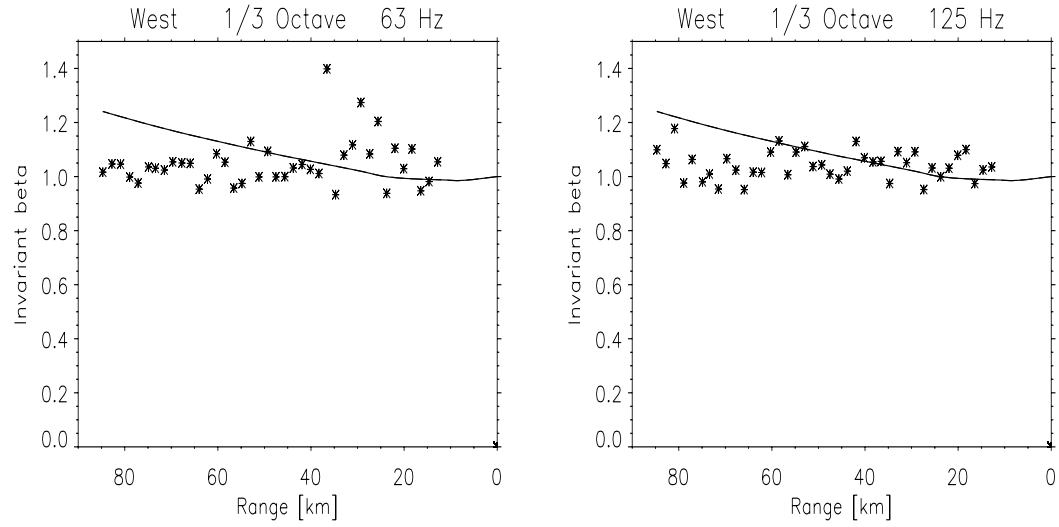

(c) 63 Hz (d) 125 Hz

Figure B.4 Western SUS run.
(a) Bathymetry (b) - (d) Invariant β as function of range
Curve: β_{theo} from bathymetry Asterisks: measured β_{meas}

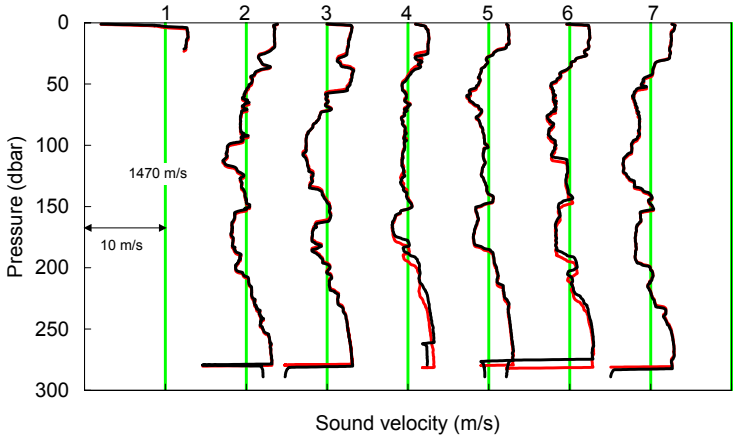

Figure B.5 Sound velocity profiles taken at the receiver

C SEARCH FOR STRIATIONS

C.1 Striations on narrowband lines

The tanker signature as shown in the lofargrams is nearly perfect in the sense that the striation patterns are very clear, and extend over a large frequency range. The broadband noise is what contributes most to this in a normal lofargram. However, in a high background noise situation such as bad weather, the broadband components of a ship's output may be overwhelmed. It is then a question of whether it is possible to observe striation patterns on narrowband lines only. The present target should be ideal for a test in this respect, as the number of lines/harmonics is large. Such a test is shown in Figure C.1. It is composed of harmonic lines only. The striation patterns are still clear.

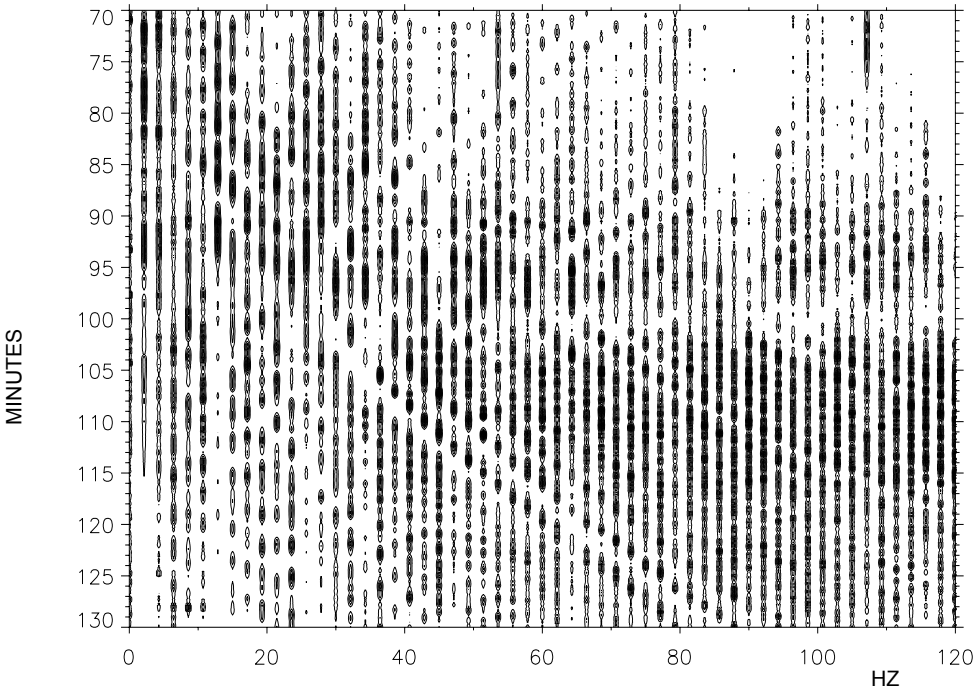

Figure C.1 Modified lofargram showing striations on strong lines

C.2 When the lines are few

If the number of lines is small, which is often the case, the task of finding striations is more difficult. Visual inspection of lofargrams over short times does hardly reveal patterns, as the striation periods are long, typically 2 – 5 minutes. It is then difficult to assess where the striations run. One could ask if more sophisticated signal processing techniques could be used. The answer to this could easily require a study of some magnitude and is considered outside the scope of this report. But a few examples can point at signal structures and characteristics that might be of relevance. The clue is to use high resolution in frequency and direction. Some reflections about the processing methods will be made. At the outset, two key questions can be asked. When observing two frequency lines,

(a) Do they belong to one and the same target?
(b) If so, where are the striations?

In this respect the parallelism in the dynamics of the lines is important, such as

(i) The systematic changes (trends)
(ii) The quasi-systematic fluctuations
(iii) The random fluctuations

The systematic component. This is caused by the target's slow changes in bearing and doppler frequency. It will mainly be useful in identifying lines belonging to the same target.

The quasi-systematic component. Spread in frequency of a line or spread in bearing is not itself necessarily a random effect. In a waveguide, a "line" is composed of several mode signals, which have slightly different bearings and different doppler frequencies. What can be modelled in this way by the waveguide equation without introducing any random elements can be considered to constitute the quasi-systematic part of the signals. But such spread can sometimes be apprehended (falsely) as purely random effects. The quasi-systematic fluctuations should in principle be useful for identifying and combining striation maxima or minima.

The random component. Purely random fluctuations are caused by influences that in practice are beyond reach of the waveguide equation. They can be caused by the source through the ship's random movements and its non-point-source character. They can be caused by irregularities in the sound velocity profile, surface waves, varying bottom topography and composition. In that case, these influences upon the received signals should *not* be expected to be connected at widely separated times, but appear more or less simultaneously at all frequencies. Thus by argument, these random fluctuations can be dismissed as clues to the identification of striations. However, random fluctuations might be useful in determining whether two lines belong to the same ship or not.

In the balance. That signal components at widely separated frequencies and times are somehow connected, is demonstrated by the presence of striations. They are the results of the above defined quasi-systematic influences. However, when regarding only two or a few signal components, the real random effects easily dominate the short-time behaviour. The prospect of answering question (b) above positively for say two lines, therefore does not seem too good.

C.3 High frequency resolution

Figure C.2 shows high resolution spectra for six consecutive harmonics over the period 100 – 130 minutes. The frequency resolution is chosen such that both the slow trends and the frequency fluctuations are emphasized. Points that belong to the same striation pattern are suggested. A slow average trend towards lower doppler is recognizable at all frequencies. Parallelism in the fast wiggles can sometimes be seen, but is often absent.

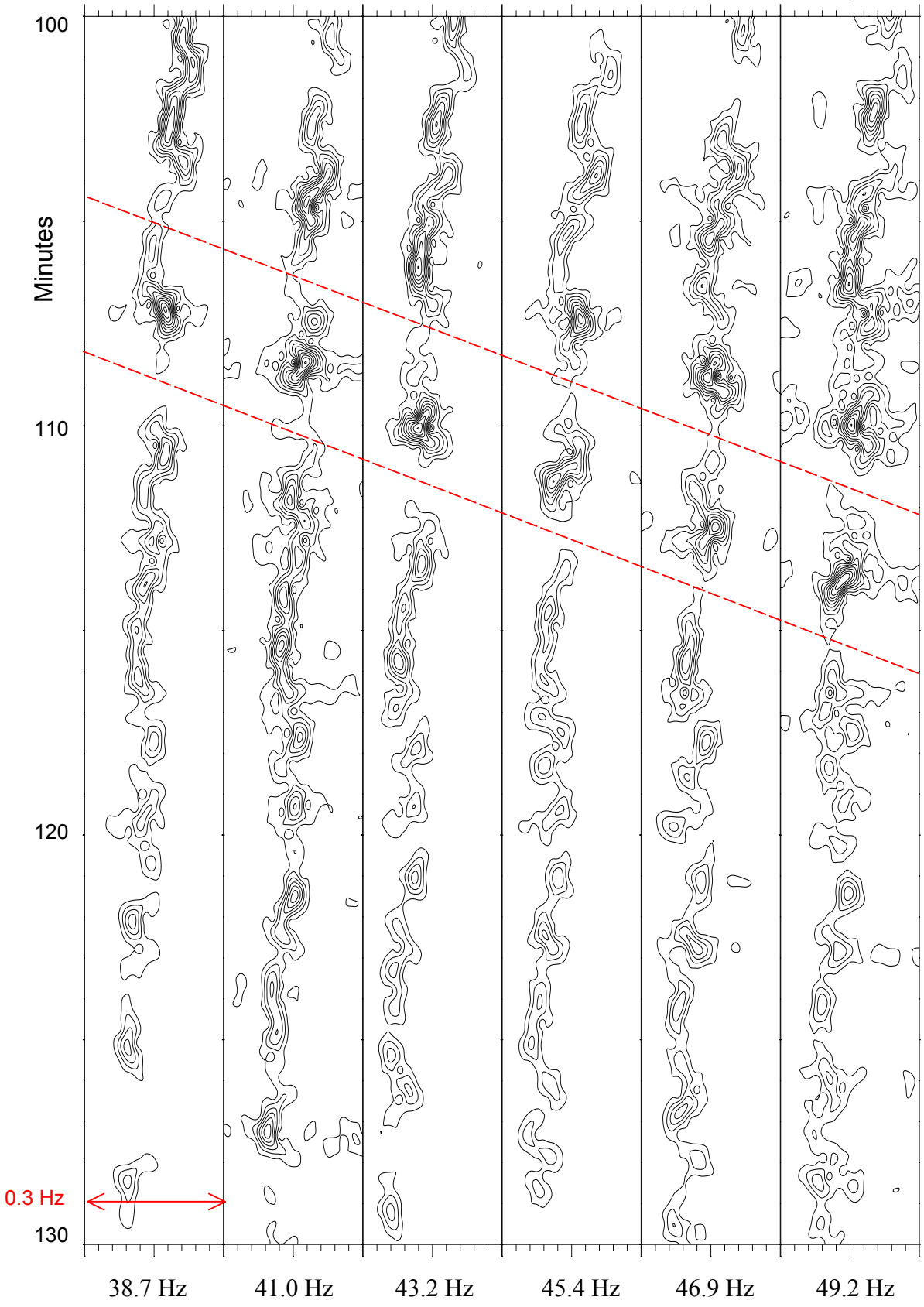

Figure C.2 Spectra for six consecutive harmonics.
Frequency resolution = 30 mHz.
Red lines indicate approximate striation minima

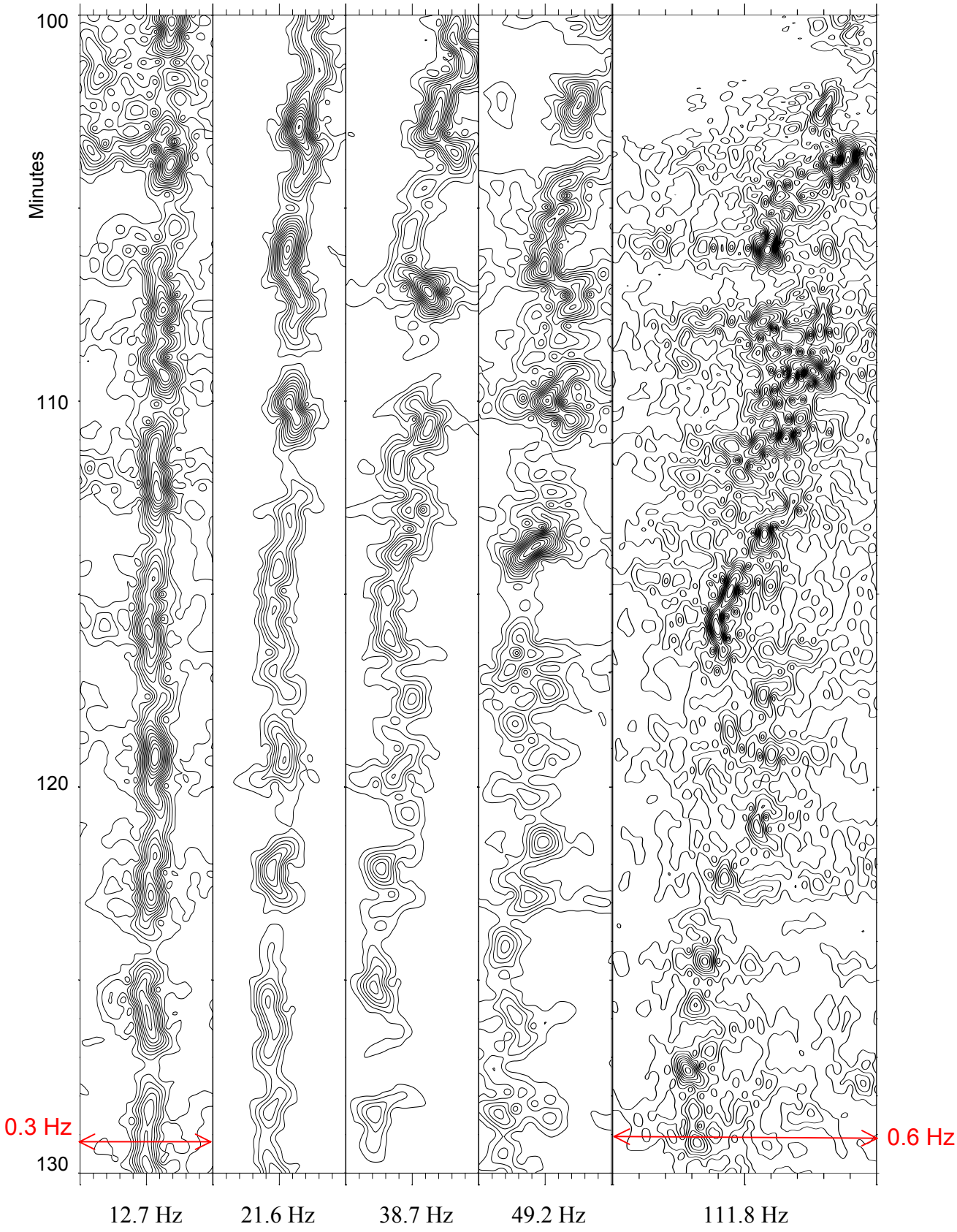

Figure C.3 Spectra for five widely spaced harmonics. Frequency resolution = 30 mHz.

Even then, as far as signatures go, this is an exceptional situation. It is not common to find many harmonics or lines so close together. Figure C.3 shows harmonics with wider spacings. Striation minima are difficult to identify. The systematic doppler trend is clear, but the fluctuations are more independent of each other than in the former case. Not much commonality can be seen. There is a spectral broadening of the fluctuations as the frequency increases.

Commonality in fluctuations should most likely occur when two lines are very close together. A somewhat rare case is shown in Figure C.4. The 30.2 Hz is a harmonic, but the 29.6 Hz is an auxiliary line that does not belong to the harmonic set. Some similarities in the variations can be seen, but there are still differences.

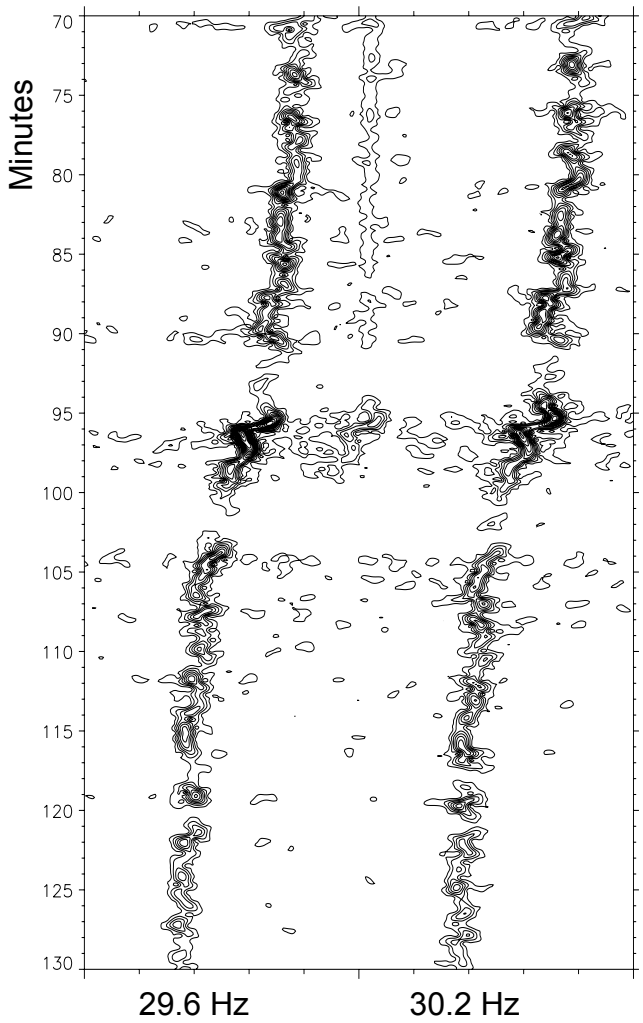

Figure C.4 Spectrum for two close lines.
Frequency resolution = 0.04 Hz.

A way of processing referring to the questions (a) and (b) above can be

(a) Search for lines belonging to the same target. Correlating pictures of the kind shown in Figures C.2-C.4 at zero time shift. Frequency axes should be scaled, in order to compensate for doppler broadening. Such processing makes indirectly use of the phase information in the signals, as this will be manifest in the frequency trends and variations. The correlator output would reflect if confidence could be attached to the outcome.

(b) Search for positions of striations. Same as above, but at different time shifts (up to minutes), after removing the slow trends. This could be a rather complicated procedure, however. A much easier way, but maybe not so good, is simply to correlate envelopes at different time shifts, possibly combined with stretching or shrinking of one of the time axes. It calls for relatively long integration times. "Envelopes only" means cutting out the phase information in the harmonics, but after it has done its work and formed the striation.

C.4 Directional spectra

Figure C.5 parallels figure C.2, showing directional (beam) spectra for the same frequency set and time period. Here a systematic directional trend is easy to see. Fluctuations in direction are less apparent. A couple of striation patterns are suggested.

Figure C.6 parallels Figure C.3. Striation patterns can hardly be recognized. Because of fixed array length, there is a broadening of the signatures towards lower frequencies.

Figure C.7 shows the time interval 115 – 145 minutes with a smaller angular span. It is now possible to see the directional spectra in more detail and one might look for resolved modes. However, there is not much consistency over time.

In searching for commonality and striations, correlation processing can be similar to that above, except for scaling of the horizontal axis. The "envelopes only" processing would be identical.

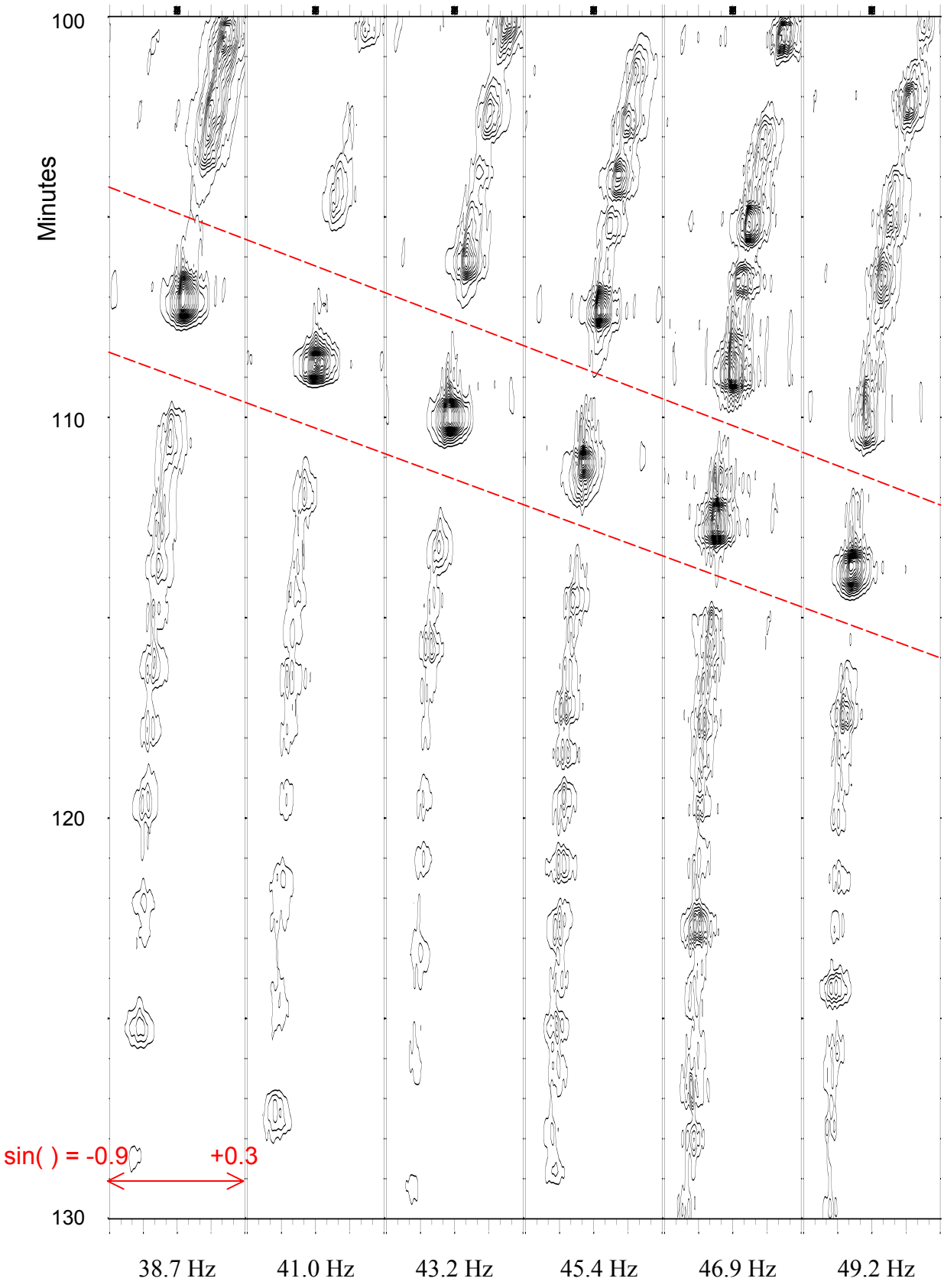

Figure C.5 Directional spectra for six consecutive harmonics sin(θ) from –0.9 to +0.3 (-64° to +17°). Red lines indicate approximate striation minima

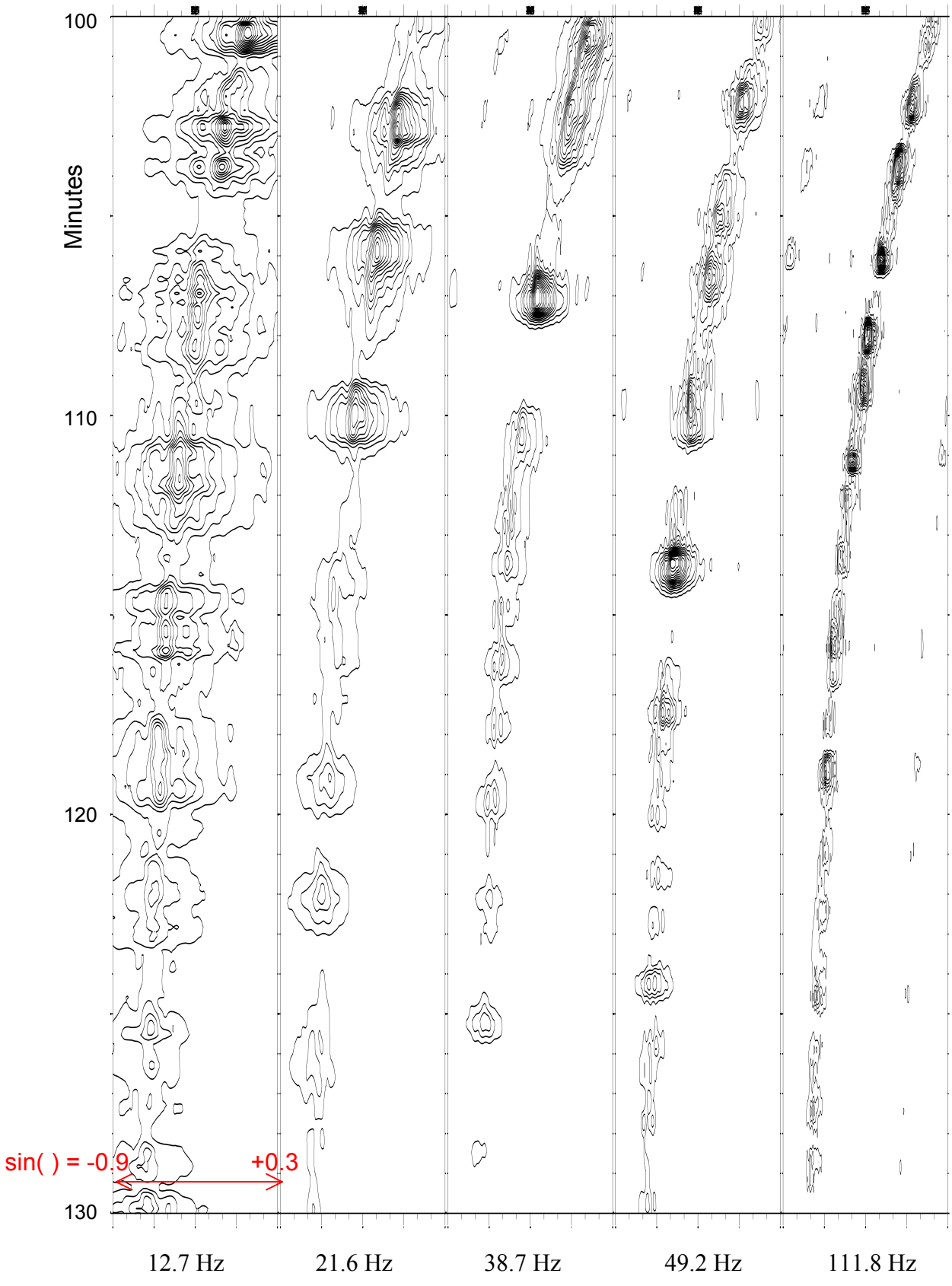

Figure C.6 Directional spectra for five widely spaced harmonics sin(θ) from –0.9 to +0.3 (-64° to +17°).

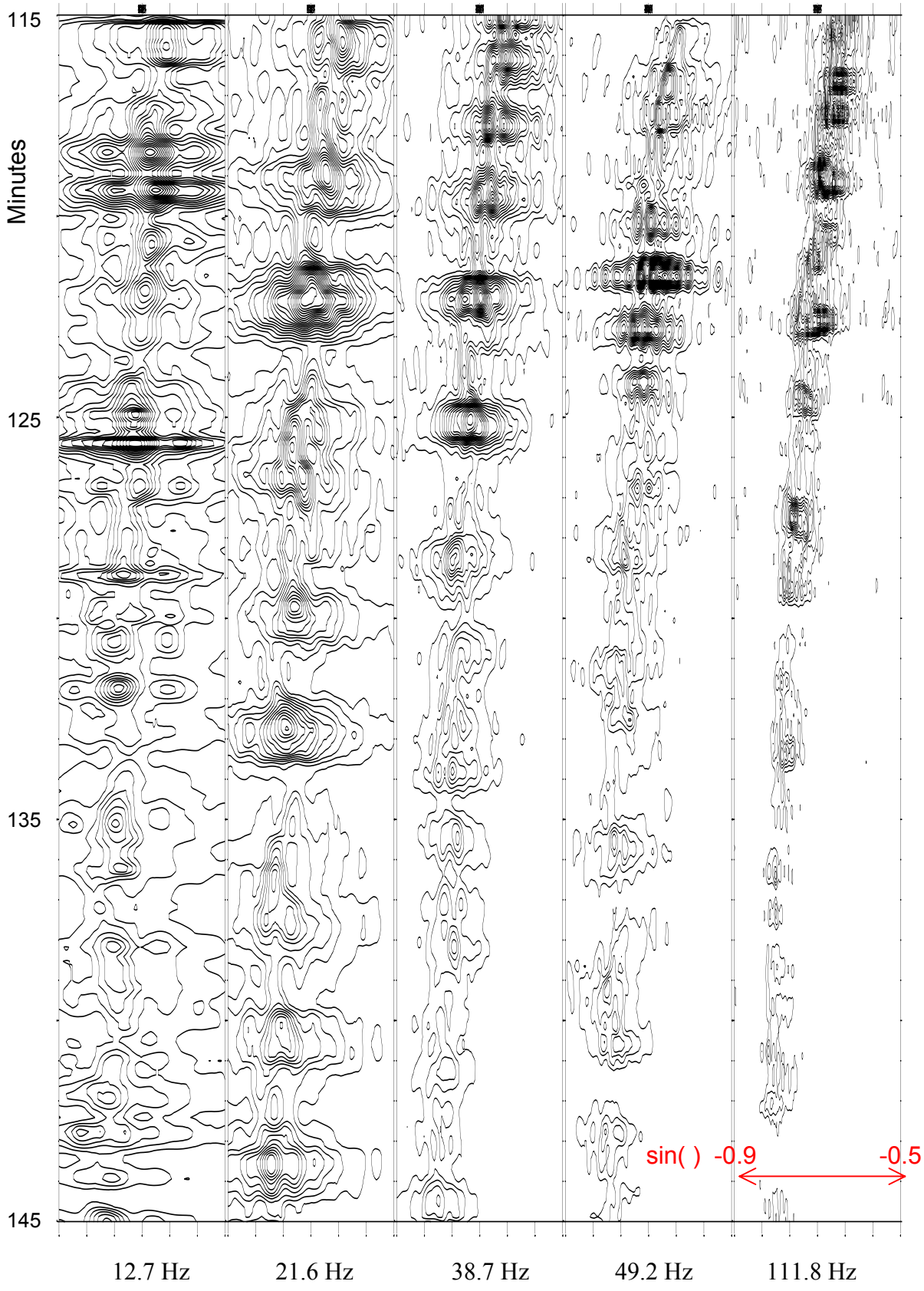

Figure C.7 Directional spectra for five widely spaced harmonics. sine(θ) from –0.9 to -0.5 (-64° to -30°).

C.5 Combining frequency and direction?

Frequency and direction for individual lines can be computed simultaneously into 2D spectra as functions of time. Instead of correlating pictures, 3D “bodies” can be correlated. If there is some connection between doppler and bearing (in theory there is, if belonging to the same target), there might be some gain.

D A 40 HZ TOWING

In Figure 1.1 there is indicated an east going track with a 40 Hz CW towed source. The run was strictly endifire, and went at 5 knots for more than 9 hours, to about 85 km. The source could be seen in spectrograms for the whole stretch (not shown). Striation speeds according to the method of Chapter 6 were possible to read off until about 40 km.

Figure D.1 shows detailed doppler spectra for the first two hours. An 8.6 second Hanning window gives a frequency resolution of 4 mHz. Similar towings in the past (7), (8) have given persistent mode spectra over periods up to ½ hour, where doppler of individual modes could be seen. Such persistency cannot be seen in the present towing. The doppler distribution seems to vary more or less randomly within the band.

Figure D.2 shows directional spectra for the same two hours. The signature shows typically a bundle of 2-5 strong arrivals plus some weaker. They are not very stable, though. Looking askew at the diagrams from below reveals a sort of Christmas-tree structure. Explanations have not been attempted.

The striation speed method of Chapter 6 gives Figure D.3. It shows hydrophone signal envelopes versus time and hydrophone position. The crossing patterns are striations moving along the array. The striation speed can be measured, and accordingly the target speed can be estimated. The 5 knots slope is indicated.

Figure D.4 (left) shows the bathymetry. In Figure D.4 (right) the continuous line is the theoretical striation speed value Equation (6.9). As the run is strictly endfire, no correction for CPA offset or skew track is necessary. The asterisks are the measured speeds, read off Figure D.3 and its successor diagrams. The measured speeds follow the theoretical values fairly well.

The mode filtering speed estimation method of Chapter 7 has also been tried. Figure D.5 gives some examples of Doppler versus bearing patterns, and Figure D.6 a collection of speed estimates. They are slightly biased upwards, but follow the trend.

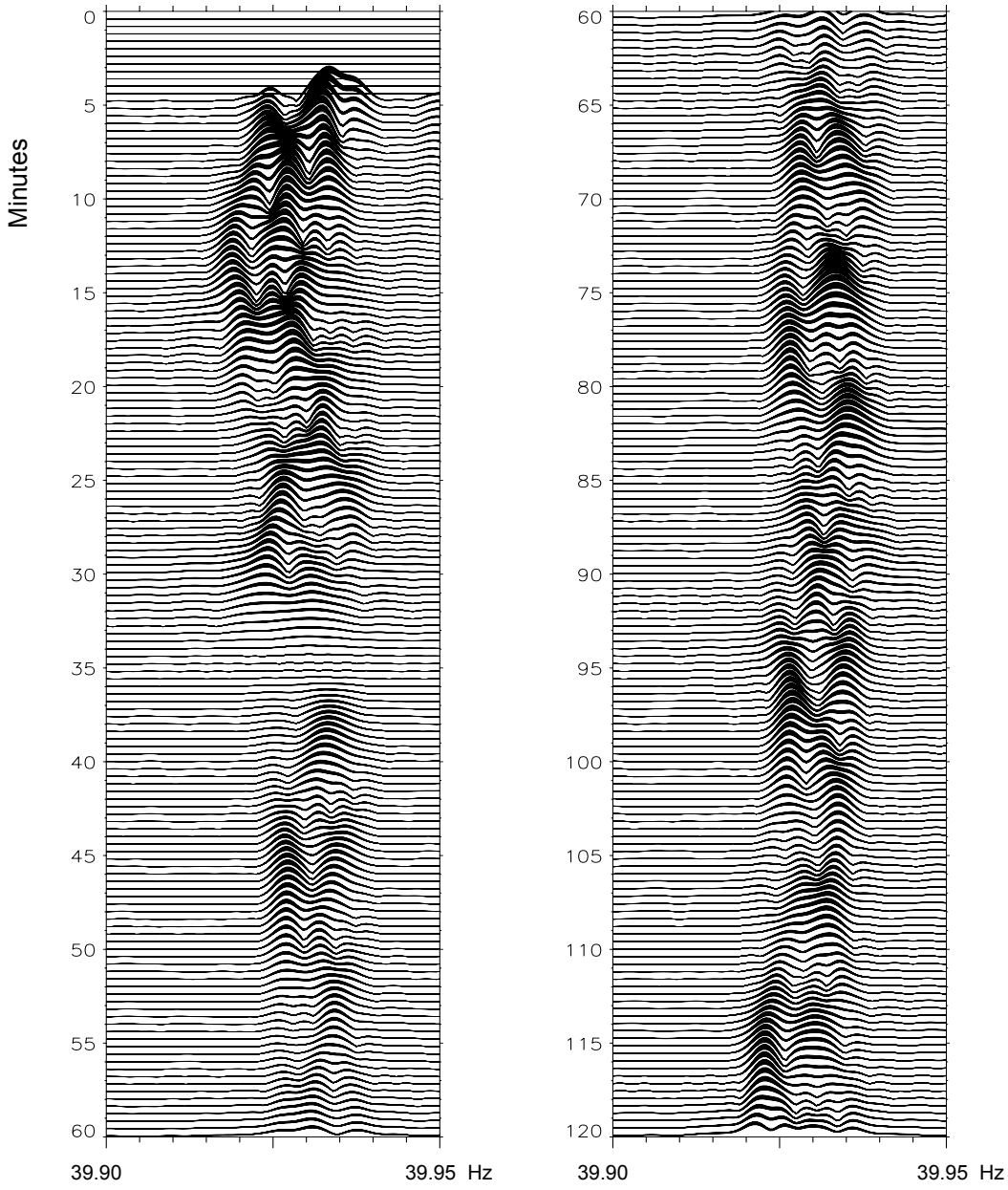

Figure D.1 Frequency spectra for towed 40 Hz source. Frequency resolution = 4 mHz

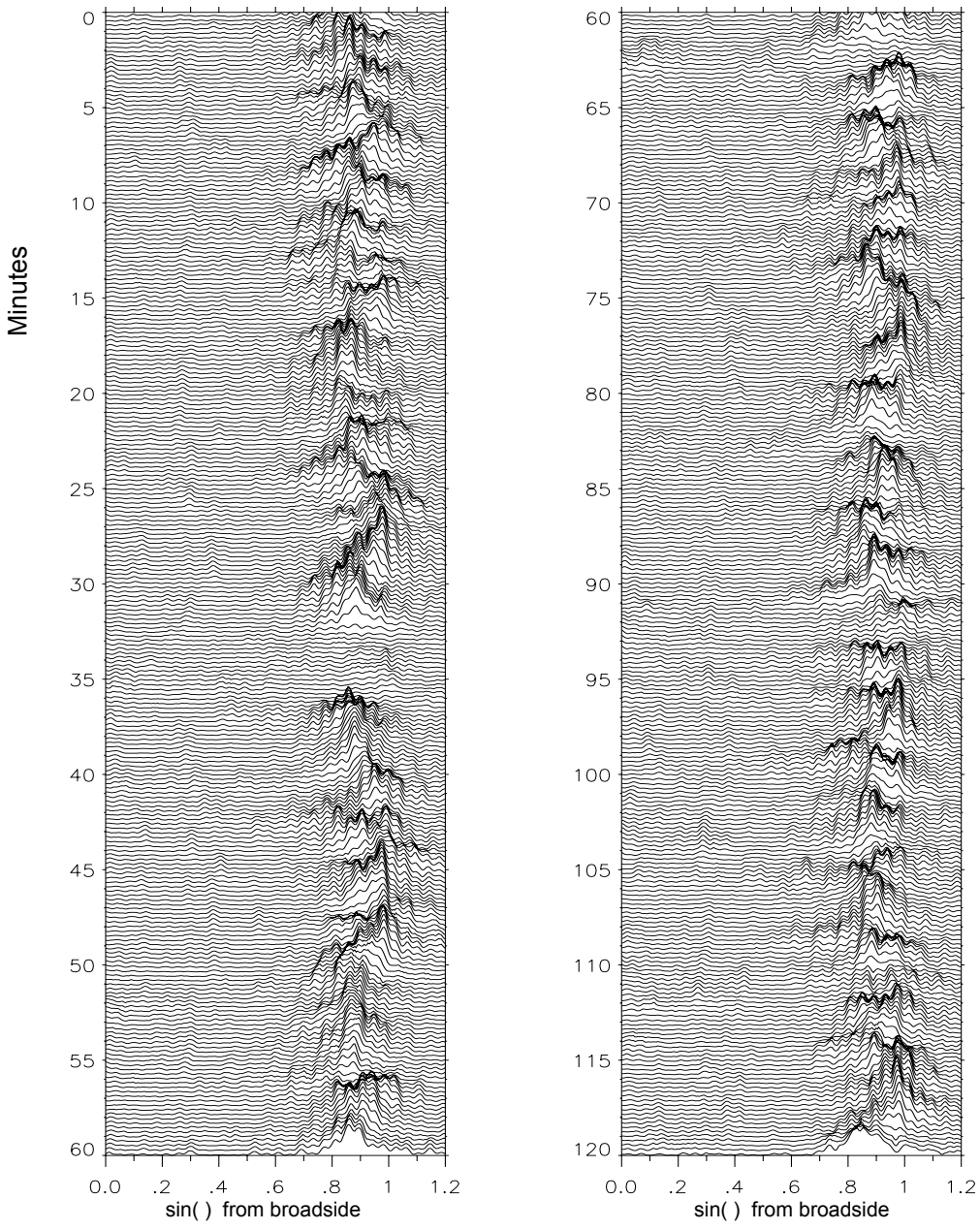

Figure D.2 Directional spectra for towed 40 Hz source
Array length 930 m

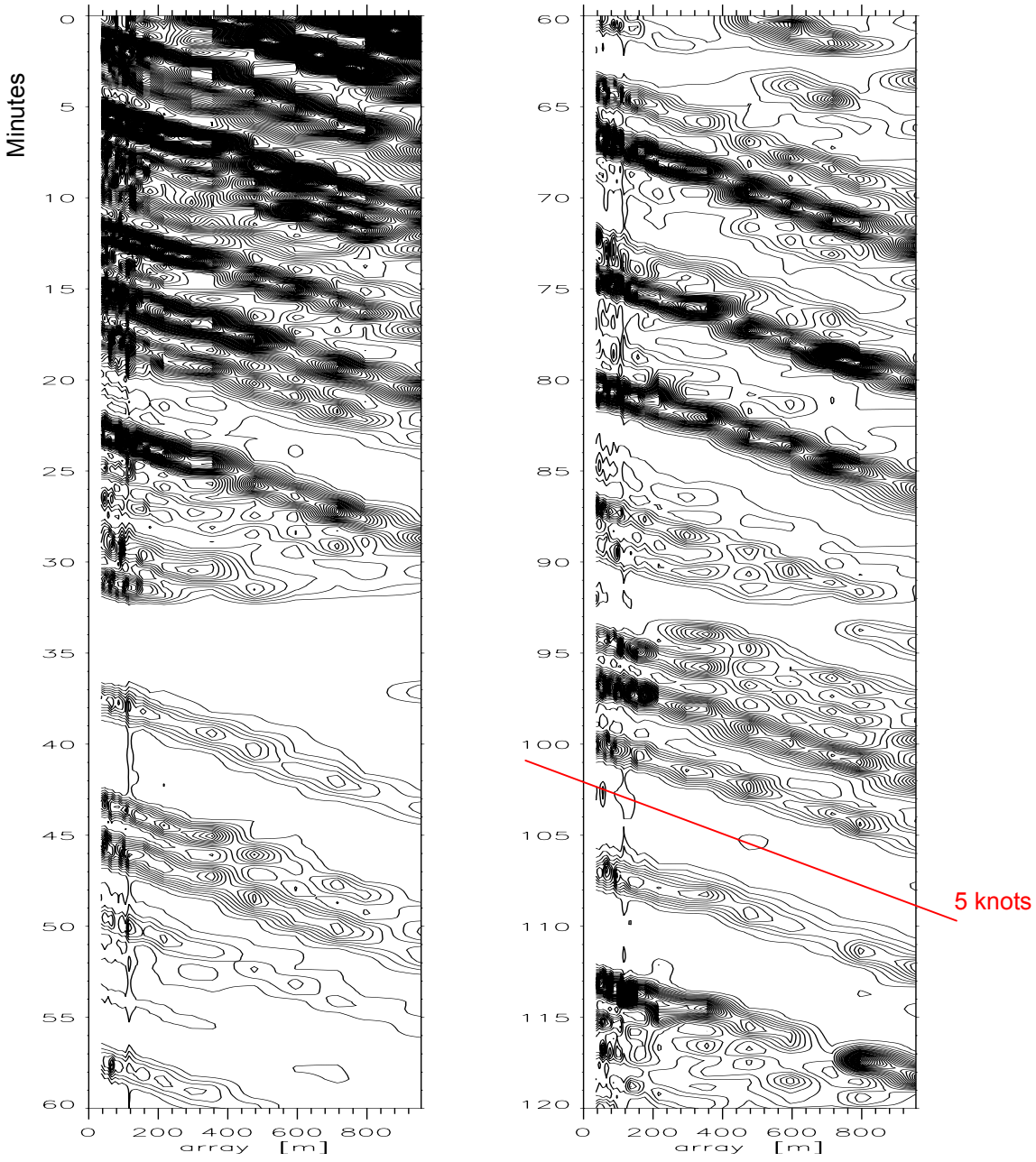

Figure D.3 Striation movement along the array for 40 Hz towed source

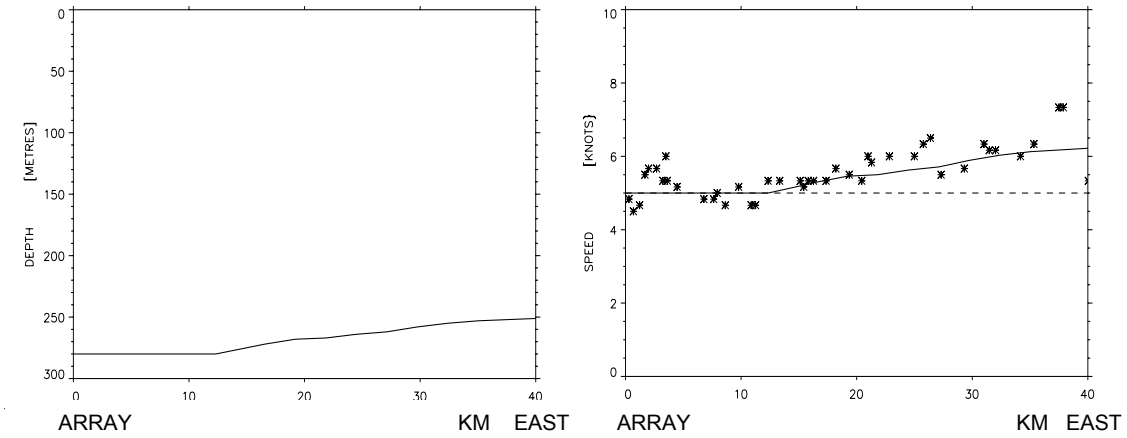

Figure D.4 Left: bathymetry for 40 Hz CW run
Right: measured striation speeds along array
compared to theoretical predictions
Continuous lines: theory Asterisks: measurements

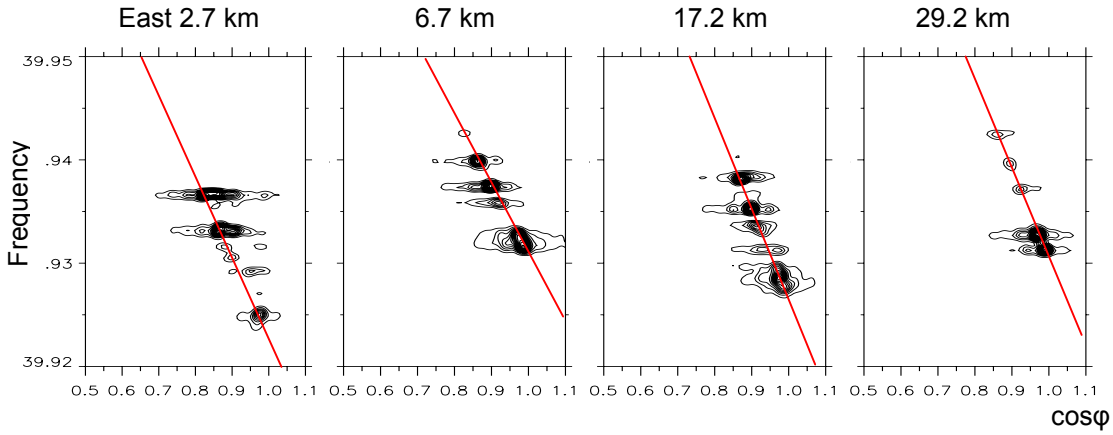

Figure D.5 Doppler frequency versus cosine of grazing angle
for 40 Hz towed source

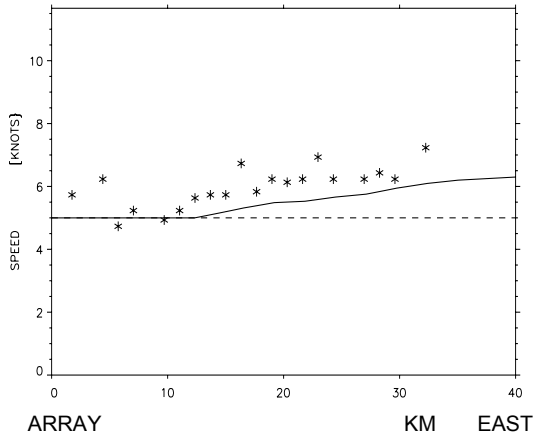

Figure D.6 40 Hz CW run. Measured speeds by the slope method
Continuous line: theory Asterisks: measurements